metals

MDPI

Review

Evaluation of Tungsten—Steel Solid-State Bonding: Options and the Role of CALPHAD to Screen Diffusion Bonding Interlayers

Ishtiaque Karim Robin [1], Tim Gräning [2], Ying Yang [2], Syeda Bushra Haider [1], Eric Andrew Lass [1], Yutai Katoh [2] and Steven John Zinkle [1,2,*]

[1] Department of Materials Science and Engineering, The University of Tennessee, Knoxville, TN 37996, USA; irobin@vols.utk.edu (I.K.R.); sbushrah@vols.utk.edu (S.B.H.); elass@utk.edu (E.A.L.)
[2] Oak Ridge National Laboratory, Materials Science and Technology Division, Oak Ridge, TN 37831, USA; graeningt@ornl.gov (T.G.); yangying@ornl.gov (Y.Y.); kathoy@ornl.gov (Y.K.)
* Correspondence: szinkle@utk.edu; Tel.: +1-208-757-1031

Abstract: Critical aspects of innovative design in engineering disciplines like infrastructure, transportation, and medical applications require the joining of dissimilar materials. This study investigates the literature on solid-state bonding techniques, with a particular focus on diffusion bonding, as an effective method for establishing engineering bonds. Welding and brazing, while widely used, may pose challenges when joining materials with large differences in melting temperature and can lead to mechanical property degradation. In contrast, diffusion bonding offers a lower temperature process that relies on solid-state interactions to develop bond strength. The joining of tungsten and steel, especially for fusion reactors, presents a unique challenge due to the significant disparity in melting temperatures and the propensity to form brittle intermetallics. Here, diffusion characteristics of tungsten–steel interfaces are examined and the influence of bonding parameters on mechanical properties are investigated. Additionally, CALPHAD modeling is employed to explore joining parameters, thermal stability, and diffusion kinetics. The insights from this research can be extended to join numerous dissimilar materials for specific applications such as aerospace, automobile industry, power plants, etc., enabling advanced and robust design with high efficiency.

Keywords: diffusion bonding; tungsten; steel; fusion plasma facing materials (PFM) design; dissimilar materials joining; CALPHAD

check for updates

Citation: Robin, I.K.; Gräning, T.; Yang, Y.; Haider, S.B.; Lass, E.A.; Katoh, Y.; Zinkle, S.J. Evaluation of Tungsten—Steel Solid-State Bonding: Options and the Role of CALPHAD to Screen Diffusion Bonding Interlayers. *Metals* **2023**, *13*, 1438. https://doi.org/10.3390/met13081438

Academic Editor: Hao Jiang

Received: 15 July 2023
Revised: 5 August 2023
Accepted: 7 August 2023
Published: 10 August 2023

Copyright: © 2023 by the authors. Licensee MDPI, Basel, Switzerland. This article is an open access article distributed under the terms and conditions of the Creative Commons Attribution (CC BY) license (https://creativecommons.org/licenses/by/4.0/).

1. Introduction

Technological advancement depends on the complex design of superior materials. The effectiveness of such design requires a site-specific material distribution and this often calls for a proper solution of joining two or more materials that is capable of providing the necessary mechanical and microstructural integrity of the design [1]. One such design is the structure of fusion reactors. Fusion reactors are potentially capable of meeting the need of the ever-increasing energy demand while keeping the environment pollution-free owing to its fuel abundance, zero carbon emission, and potential for economical operation [2,3]. However, several issues need to be addressed in order to make it feasible to generate energy from fusion reactors in a safe manner [4]. One of the major problems is the joining of plasma facing materials and structural materials of fusion reactors [5–8] Among the plasma facing materials (PFM), tungsten is considered to be the most promising candidate material. Some of tungsten's major advantageous mechanical properties include high melting temperature, high thermal conductivity, low vapor pressure, low tritium retention, high sputtering resistance, and so on [9–11]. However, being a brittle material at room temperature and with a high ductile brittle transition temperature, tungsten is not capable of providing structural integrity for the reactor [12,13]. As a structural material, ferritic/martensitic (FM) steel is one of the best candidate materials owing to its superior mechanical properties

capable of providing structural integrity [14]. Therefore, it is necessary to find a suitable solution for joining tungsten and ferritic/martensitic steel.

Even though numerous studies with different designs and approaches have been explored to join tungsten with steel [15–17], an effective and real-life applicable method to join these two materials is yet to be found. Some major issues of joining tungsten with steel are the difference between melting temperatures (1550 °C for FM steel vs. 3400 °C for W) which prevents conventional welding, a large difference in coefficients of thermal expansion (CTE) (12×10^{-6} K^{-1} for FM steel vs. 4.4×10^{-6} $K^{-1}$for W), and formation of brittle intermetallic phases like Fe_7W_6 (μ-phase) [18–21]. A proper joining of tungsten and steel may require the introduction of multiple interlayers in between them which would help to lower the mechanical property gradient along the joining interfaces and prevent the formation of brittle intermetallics. CALPHAD (CALculation of PHAse Diagram) modelling, which plays a crucial role in understanding complex materials' systems under different conditions, has been leveraged for a better understanding of tungsten steel joining [22]. CALPHAD is a widely used computational approach in materials science to predict phase equilibria in multi-component systems [23]. It utilizes thermodynamic databases containing Gibbs energy data for phases as a function of temperature, pressure, and composition. Thermo-Calc (version 2022a), with the TCFE9 database, was employed in this review paper to generate accurate phase diagrams, offering insights into phase stability and composition in different alloy systems [24,25]

In this work, a systematic approach was followed to compile and critically review data from different studies investigating the solid-state diffusion joining of tungsten and steel. The primary objective is to address the challenge of integrating structural materials and plasma-facing materials in fusion reactors. Thermodynamic reactions between interlayers with tungsten and steel at various temperatures and their feasibility for fusion reactor applications were also discussed. Understanding diffusion characteristics for the entire transition layer configuration at service-relevant and manufacturing temperatures, regardless of the bonding technique employed, is of paramount importance. This review serves to compare and contrast published data on the solid-state joining of tungsten and steel, laying the groundwork for potential viable joining solutions in real-life fusion reactor applications. Moreover, the work proposes a new paradigm for solid-state diffusion bonding between diverse materials with broader applications in aerospace, automobile, power plants, and other fields where solid-state bonding plays a crucial role in design, providing enhanced efficiency and reduced environmental impact.

2. Mechanism of Diffusion Bonding

Understanding the atomic bonding formation through the interaction of atoms during diffusion is of paramount importance when investigating solid-state bonding in materials. The diffusion process is determined by the kinetics of atom migration through surface, grain boundary, or bulk matrix [26,27]. Manufacturing process parameters such as temperature [28], pressure [29], holding time [30], surface roughness [31], and activation layers play a key role in the formation of the bond [32–34]. While investigating the joining of different configurations of tungsten and steel, one must pay careful attention to the process parameters and diffusion kinetics to have a good understanding of why different parameters yield different microstructural and mechanical properties.

2.1. Diffusion Bonding Overview

The definition of diffusion bonding provided by Kazakov [35] has been adopted by the International Institute of Welding (IIW): "Diffusion bonding of materials in the solid state is a process for making a monolithic joint through the formation of bonds at atomic level, as a result of closure of the mating surfaces due to the local plastic deformation at elevated temperature which aids interdiffusion at the surface layers of the materials being joined". Diffusion bonding between two mating surfaces goes through three steps which are schematically shown in Figure 1 [36]. In the first step of diffusion bonding, asperities

from one mating surface exert force on another mating surface, which results in localized plastic deformation at the bonding temperature. Brittle oxides on the surface are fractured and metal-to-metal contact is established. In the second step, the thermally activated migration of atoms between two mating surfaces leads to the atomic diffusion between the surfaces and the production of a bond. In the final step, elimination of the majority of pores occurs and a homogenized bond is produced [37]. A reaction layer is produced in the interface, and process parameters dictate the characteristic of this reaction layer. A large difference between diffusivity of major alloying element from the mating surfaces can result in Kirkendall pores and degrade the mechanical properties of the joint [38]. In a tungsten–steel transition layer configuration, the presence of chromium and aluminum often results in the formation of a passivation oxide layer [39,40]. Therefore, care should be taken while determining process parameters like temperature and pressure so that these oxide layers can be eliminated and contact between the mating surfaces is established.

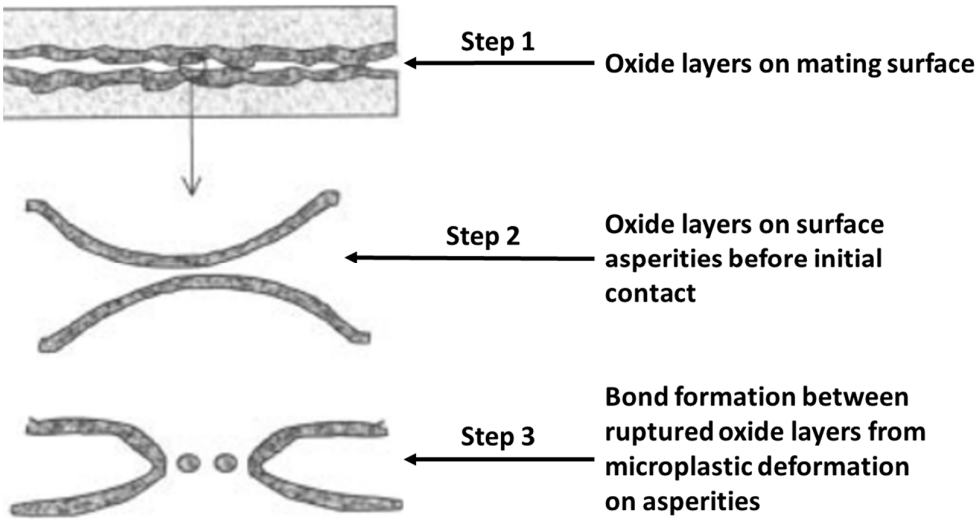


Figure 1. Steps of forming diffusion bonding between two surfaces. Figure modified from Ref. [36], 2001 with permission from John Wiley and Sons.

2.2. Advantage of Diffusion Bonding over Welding

The near net shape process of diffusion bonding has been explored widely because of the flexibility to choose a combination of elemental compositions while avoiding the formation of brittle intermetallic phases at the interface [38]. It is also possible to suppress elemental segregation in diffusion bonding and maintain a relatively low residual stress in comparison to other non-solid-state welding processes [41–44]. Diffusion bonding stands out among various joining techniques due to its minimal temperature gradient in the joint in comparison to other methods. Elimination of a heat-affected zone (HAZ) and highly complex microstructure from non-equilibrium phase transformation and chemical segregation during melting is possible via solid-state diffusion bonding, which makes it a lucrative option to be employed for joining in different industrial sectors like aerospace [45–49], fusion reactor concepts [3,50–54], plate type heat exchangers and reactors [55–62], and so on [26].

2.3. Atomistic Model of Diffusion

The atomic diffusivity is given by the following Equation (1), which represents the increase in diffusivity with the increase in temperature [26,63]:

$$D = D_o \exp\left[\frac{-\Delta E_{act}}{\mathrm{RT}}\right] \quad (1)$$

Here, D is the diffusivity (m^2/s), D_o is the frequency factor (m^2/s), E_{act} is the energy of vacancy formation and migration (J/mol), R is gas constant, and T is temperature in Kelvin. The thickness of the reaction layer (x) in a diffusion couple is estimated by the following Equation (2) [64].

$$x = kt^n \tag{2}$$

where k is a rate constant, t represents time, and n is a kinetic exponent. This equation is based on the solution of Fick's second law. For interfacial diffusion, grain boundary diffusion, and volume diffusion, the value of n is 1, 0.5, and 0.25, respectively [65–67]. In other words, the different values of n come from different diffusion pathways.

2.4. Important Parameters for Diffusion Bonding

2.4.1. Temperature

The most significant factors to influence the diffusion bonding are bonding temperature, bonding pressure, and holding time. As it can be seen in Equation (3), the diffusivity is a function of temperature and it is assumed to follow an Arrhenius-type relation which can be shown in the following equation where the rate constant k from Equation (2) is presented as a function of temperature [68].

$$k = k_o \exp\left[\frac{-E_a}{\mathrm{RT}}\right] \tag{3}$$

where k_o is the pre-exponential factor and E_a is activation energy of reaction layer growth. A rise in the temperature tends to increase the thickness of the reaction layer [28]. With the temperature rise, there is an increase in diffusivity and the diffusion coefficient can be doubled even for a moderate rise of 20 °C [63].

2.4.2. Pressure

A minimum amount of bonding pressure is required for proper diffusion bonding at a particular temperature. The applied pressure is responsible for the first step of diffusion bonding where force is exerted on asperities to produce deformation and eliminate oxide layers. Several studies pointed out that a rise in pressure to moderate values results in a higher bond strength [69–71]. A few studies discussed impulse pressure-assisted diffusion bonding where varying pressure is used during diffusion bonding instead of a constant pressure and it was claimed that the overall processing and bonding time was reduced through the use of impulse pressure-assisted diffusion bonding [29,72–78].

2.4.3. Holding Time

The holding time is another very important parameter for determining the strength of diffusion bonding as it can be understood from Equation (2). In previous studies [30,79–82], an increase in holding time increased the strength of the bond. Time is required to fill up the pores in the mating surface in order to establish a sound bond. Sufficient pressure at high temperatures causes deformation and holding time needs to be controlled in order to have the desired mechanical properties in the bond. A long heating time often results in excessive loss of intermediate layers and, as a consequence, a significant deterioration of the dissimilar materials' joint, which produces a weaker bond. On the other hand, if the holding time is too short, then there may be insufficient solid-state diffusion, which would also cause a weaker bond. Models have been developed that can estimate the required time for proper diffusion bonding. For example, Li [83] developed a probabilistic model using Fick's diffusion law for the necessary time to ensure sufficient diffusion. By following Equation (4), total bonding time t can be estimated.

$$t = \int_{f_0}^{f} \frac{-\sigma_e/\dot{\epsilon}}{\left((3p\sqrt{f} - \frac{2\gamma\sqrt{f}}{r_o} + \frac{6\gamma}{r_o}) + \frac{2{r_o}^2 p}{\ln(\frac{1}{f}) - \frac{1-f}{2}} \frac{\Omega}{KT}\left[\frac{1+\frac{h}{d}}{h} D_{\mathrm{gb}}\delta + 2\Omega D_{\mathrm{v}}\right]\right)} \mathrm{df} \tag{4}$$

Here, Ω is the atomic volume; D_{gb} is the grain boundary diffusivity; D_v is the volume diffusivity; and δ, d, and h are grain boundary width, grain size, and void height, respectively. r_0 is the initial void radius or surface roughness, r is the instantaneous void radius, $f = (\frac{r}{r_o})^2$, γ is the surface energy, σ_e is the Levy–Mises effective stress, $\dot{\epsilon}$ is the effective plastic strain rate, K is the Boltzmann constant, p is the external pressure, and T is the temperature in Kelvin.

2.4.4. Other Diffusion Parameters

Other important factors that influence the diffusion bonding are surface roughness and passivation layers. Larger asperities need to be removed in order to create a sound bond [58,59]. A good surface finish is desired because the initial contact area largely depends on the presence of asperities and voids on the mating surfaces [80]. However, a contradictory result was found by Zuhuri [31], where it is shown that a rougher surface yielded a better tensile strength of the bond. As a possible explanation, it was mentioned that a rougher surface would have more asperities and, therefore, exerted pressure would be more localized to result in higher force that will eventually cause a higher diffusion between the mating surfaces. A surface roughness of 0.84 µm produced a maximum ultimate tensile strength (UTS) value of ~130 MPa, while a surface roughness of 0.18 µm produced a UTS value of ~80 MPa for the bonding of aluminum alloys. On the other hand, tensile strength and joint efficiency were improved with a smoother surface finish [84,85]. The tensile strength of the joint of a Cu-Cu (copper-copper) couple was found to be ~50 MPa and ~5 MPa for surface roughnesses of 90 nm and 1.5 µm, respectively, for a bonding temperature of 400 °C and 20 min bonding time. It was also suggested that a higher pressure is required for a superior bonding when the surface roughness is high [86]. The passivation layer becomes an issue for materials like aluminum, stainless steel, nickel, and titanium alloys where a thin oxide layer prevents further oxidation of the materials, resulting in good corrosion resistance [63]. For materials like titanium, it is possible to dissolve the passivation layer in the matrix material [48]. For other materials, processes like chemical pickling or sputtering with argon ions can be used to remove passivation layers [63].

3. Historic Overview of Refractory Alloy Joining

Joining of refractory materials such as tungsten, molybdenum, tantalum, and niobium was investigated by Scott and Knowleson [87] and others [88]. Tungsten, molybdenum, tantalum, and niobium are the refractory materials most often used in structural applications owing to their superior mechanical properties resulting from high melting points, high densities, low specific heats, body-centered cubic (BCC) crystal structure, and low coefficients of thermal expansion [89]. However, W and Mo possess ductile brittle transition temperatures (DBTTs) near or above room temperature, causing these materials to be prone to brittle fracture and low fracture toughness for room temperature applications. Other factors such as impurity addition during alloying, fluctuations during strain rate, heat treatment, and processing history during manufacturing also contribute towards performance under the service condition [87,89]. The major joining processes include fusion welding such as arc welding, electron beam welding, resistance welding, and non-fusion or solid-state joining such as pressure welding, ultrasonic welding, and friction welding. Tungsten and molybdenum are typically produced through powder metallurgy, and fusion welding is generally avoided for these materials due to their low ductility which essentially becomes zero (i.e., fracture occurs in fully brittle nature) after recrystallization [87]. Joining through fusion welding requires the fulfillment of a few conditions. The surface has to be very clean prior to welding and a high purity inert gas needs to be used during the welding process. These refractory materials are very sensitive to oxygen, nitrogen, and carbon and tend to form carbides and oxides when exposed to impurities because of their very low solubility. The high melting temperature of refractory alloys leads to longer cooling times and a larger range of temperature over which thermal strains can be created

from different thermal expansions and contractions. Intrinsic characteristics of refractory materials like high modulus and yield strength and resistance to plastic flow contribute to an increase in residual stress in the weld joint. Oftentimes, a heat treatment below the recrystallization temperature is required for alleviating some of the residual stress. However, proper caution should be maintained so that grain growth is avoided; a decrease in tensile strength, ductility, and toughness and an increase in DBTT is caused by the grain growth. Solid-state joining is often very challenging for refractory materials because of the very low diffusivity and a very high required temperature (more than 50% of homologous melting temperature) along with the need to apply high pressure for the diffusion process to effectively produce a solid-state joint. Cadden and Odegard Jr. [90] discussed the possible use of brazing with filler materials like palladium–nickel or palladium–cobalt when joining refractory elements like W- and Mo-based heat sink materials. Here it was reported that successful bonding was achieved with tungsten couples, but grain boundary cracking was exhibited after the bonding. Due to the insufficient ductility and the development of secondary phases, the practical utilization of brazing is constrained. Moreover, filler materials that include Ni are prohibitive for fusion energy applications from the standpoint of neutron-induced radioactivity.

4. Tungsten and Steel Bonding without Interlayers

Research on direct diffusion bonding between tungsten and different variants of steels has been published with varying success rates. Qu et al. [91] produced functionally graded material (FGM) bonding for tungsten/iron under a high pressure of 9 GPa, where the volume fraction of tungsten was varied from 0% to 100% with a 25% interval, which resulted in a relative bond density of 97%. The formation of intermetallic Fe_7W_6 (μ phase) was observed in the transition layers and a correlation was found between the iron particle sizes and the thickness of the intermetallic layer; finer particles of Fe produced a thicker intermetallic layer. Intermetallic layers of FeW and Fe_2W were also found in a EUROFER97 steel and tungsten joint without any interlayer [92], though with the help of post-build heat treatment at 1050 °C, a high tensile strength was achieved. Interestingly, the heat treatment caused the ferritic/martensitic EUROFER97 steel to go through a full austenitization process. In Figure 2, this diffusion bonding between tungsten and EUROFER97 is shown. Oono et al. [93] joined tungsten and oxide dispersion-strengthened (ODS) steel through the means of brazing and solid-state diffusion bonding. Tungsten was found to be the major diffusion element with higher penetration depth into steel but elements from the steel side (i.e., Fe, Cr) had a very small diffusion into tungsten. Wang et al. [94] performed diffusion bonding of tungsten/copper where amorphous Fe-W was used as an interlayer and the transformation from amorphous to crystalline was observed during the bonding process. The experiment intended to avoid the formation of voids and brittle phases like Fe_2W. However, for a heat treatment at 950 °C for 60 min, Fe_2W, Fe_7W_6 (μ phase), and α-Fe phases were observed. A functionally graded transition layer between tungsten carbide (WC) and stainless steel was explored by Kawakami [95]. Pre-sintered WC alloy was bonded with 316L stainless steel via pulsed current sintering (PCS) using 20 wt% binder materials. The formation of four interlayers transitioned from 20, 40, 60, and 80 wt% of WC, and the Vickers hardness (HV) value increased from ~230 to ~1180 with the increase in WC. A summary of some of the previous works on tungsten and steel direct bonding through diffusion is provided in Table 1.

The studies presented here provide evidence that the formation of bonding between tungsten and steel through diffusion is feasible; however, it inevitably results in the formation of embrittling phases (discussed further in the next section). This is particularly problematic for applications that involve mechanical and thermal loading, where the presence of embrittling phases can render the joint unsuitable for structural use. Furthermore, the minimum homologous temperature required for tungsten diffusion induces recrystallization and grain growth in steel, which can significantly compromise the mechanical properties of the structure. These findings underscore the need to carefully consider

the implications of tungsten diffusion on the mechanical behavior of steel in structural applications.

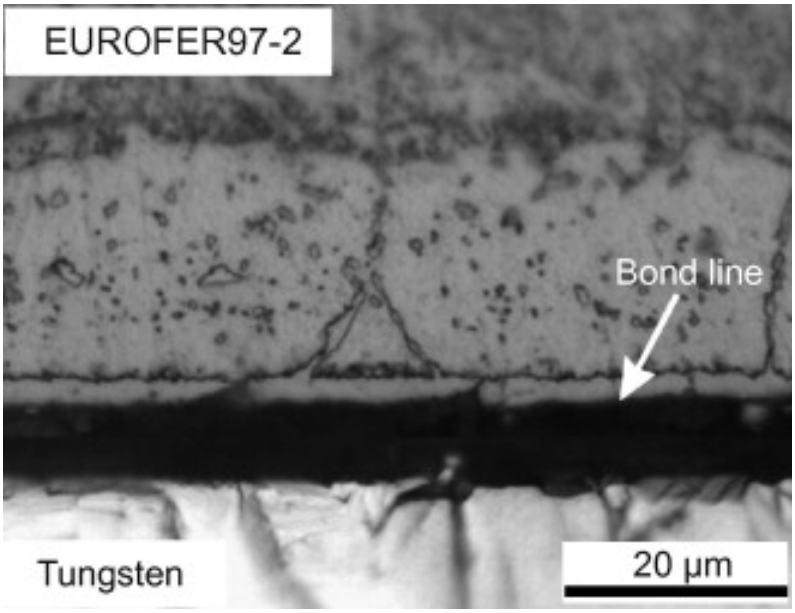


Figure 2. Scanning electron micrograph of tungsten–steel (EUROFER97-2) direct bond, reprinted from Ref. [92] with permission from Elsevier.

Table 1. Diffusion bonding between tungsten and steel without interlayers from the literature.

Bonded Materials	Bonding Parameters	Mechanical Properties	Microstructural Properties	Ref.
W and Fe	9 GPa, 11 KW for 60 s	Max hardness is ~725 HV and 500 HV for as-built and heat-treated, respectively	Brittle Fe_7W_6 formed	[91]
W with EUROFER	1050 °C + 1 h, 3 h, 4 h, PBHT ★: (1) 760 °C + 90 min (2) 650 °C + 90 min	440 MPa at 650 °C and 0.14 J/cm^2 at 550 °C Hardness 6.7 GPa on the surface of W, 2.8 GPa on the thick layer in the interface	One thin layer (2.5–4 μm) with intermetallic phase FeW, one wide layer (13 μm for 1 h and 25 μm for 4 h) with high W concentration of ~8 wt%	[92]
W with ODS steel, brazing interlayer used iron-based amorphous alloy	1180 °C, 25 MPa, 0.5 to 4 h		W diffuses significantly into steel but Cr and Fe did not penetrate W	[93]
WC and steel FGM layer sintered by PCS	Sintering pressure 20–40 MPa	Three-point bending strength ~650 MPa		[95]
W with Cu, using W-Fe amorphous interlayer	900 and 950 °C, 60 min, 30 MPa	Max tensile strength 146 MPa	Fe_2W, Fe_7W_6, α-Fe intermetallic formed	[94]

★: Post-build heat treatment.

Diffusion Kinetics between Tungsten and Steel

For a ferritic-martensitic steel where the Cr concentration is within a range from 8 to 12 wt%, a direct bond between tungsten and steel will produce brittle intermetallic phases like Fe_6W_7, which has a space group $R\bar{3}$ mH (trigonal crystalline structure) [96]. Another intermetallic that is typically common in all tungsten–steel joints is Fe_2W, which is in space group $P6_3mc$ with a hexagonal crystalline structure [97]. A ternary phase diagram of W, Fe, and Cr at 1300 °C to represent W and ferritic/martensitic steels is shown in Figure 3. The Fe_7W_6 (μ-phase) intermetallic forms due to incomplete solid solubility within the alloy system and oftentimes the interface between the bulk matrix and intermetallic acts as a crack nucleation zone [98], causing the material to be of inferior quality with lower toughness properties. With the exposure of the interface to high temperature for

an extended time, the thickness of intermetallic layers tends to grow [99], making the W-steel joint weaker as the growth of the intermetallic will have a detrimental effect on the mechanical properties. In high-temperature applications characterized by repeated thermal cycling, reducing the coefficient of thermal expansion (CTE) mismatch between dissimilar materials is crucial to accommodate thermomechanical stresses in the joint. This is essential to prevent premature failure and ensure the long-term reliability of the system. While it is possible to mitigate the issues arising from the large difference in mechanical properties between tungsten and steel to some extent through the use of concentration gradients as reported by Kawakami et al. [95], it is not possible to avoid the formation of brittle intermetallics with a direct bond between tungsten and steel at the desired operation temperature or to accommodate manufacturability. One way to resolve this problem could be the introduction of one or multiple interlayers with different compositions to avoid any brittle intermetallic shown in the phase diagrams of the associated elements. This interlayer can also reduce CTE mismatch thermal stresses, thereby enabling a smoother transition of the mechanical property difference between tungsten and steel.

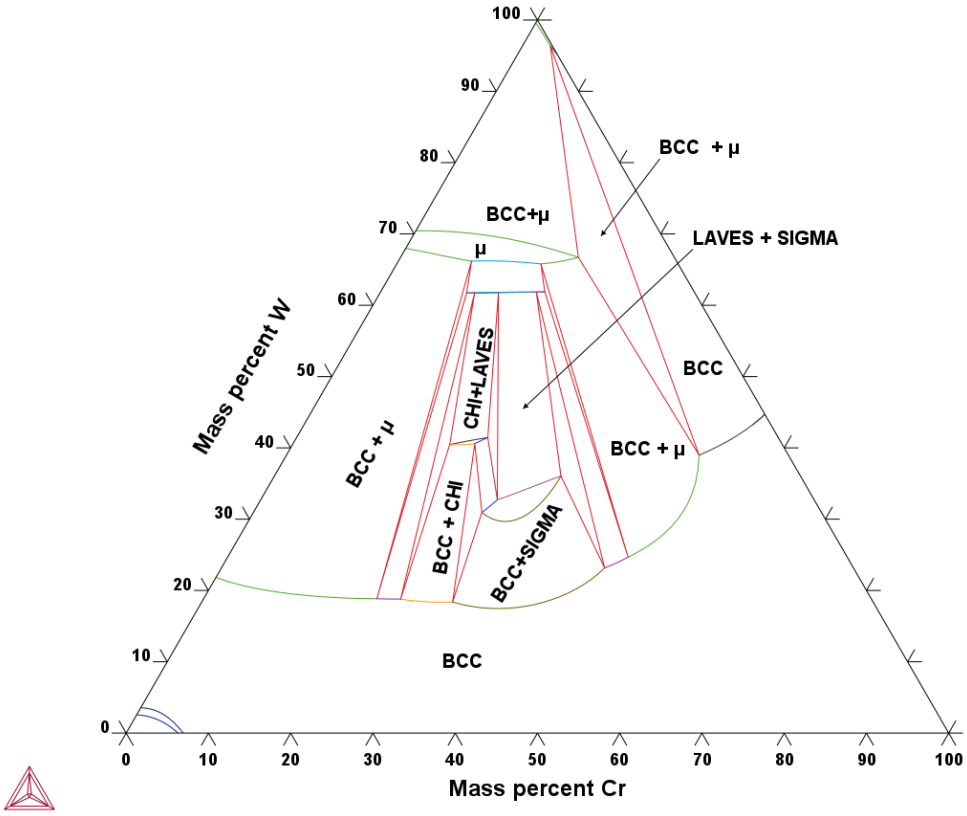


Figure 3. Fe-W-Cr isotherm phase diagram at 1300 °C (calculated from Thermo-Calc using TCFE9 database).

5. Tungsten and Steel Bonding with Interlayers

One of the biggest environmental challenges for nuclear reactors is the waste disposal when the reactor is decommissioned. Having the flexibility to dispose of materials through shallow burial would be a great advantage [100,101]. Keeping this in mind, selection of materials with low neutron-induced activation is highly desirable for a transition layer design between tungsten and steel for nuclear energy applications [102]. Materials such as copper, nickel, and niobium are relatively high in activation and possess long half-lives. Due to high activation, Ni, Mo, and Nb are removed from the variant of ferritic/martensitic steel known as reduced-activation ferritic steel [100]. Even though some of the elements cannot be used in fusion reactors due to high activation levels, these materials can be used as transitional elements where activation due to neutron irradiation is not a design variable,

like liquid metal, supersonic aircraft, and high-temperature power plant components [46]. Some potential interlayers for tungsten–steel bonding are discussed below.

5.1. Copper Interlayer

In Table 2, a few studies were summarized where copper was used as a single or a part of multiple interlayers while joining tungsten and steel. One of the major advantages of Cu is that it is a non-carbide-forming element and it can inhibit the diffusion of carbon atoms, which would otherwise facilitate the formation of carbides with elements like titanium, vanadium, etc. (commonly found in steel); mechanical properties like toughness and plasticity can be deteriorated when these carbides grow at high temperature [103,104]. Cu can also form a solid solution with Fe, Cr, and Ni without producing any brittle intermetallic compounds [105]. Copper alloys are also known to be attractive heat sink materials that can be used in high heat flux applications due to their high thermal conductivity [106]. Cu has been used, both as a single interlayer or a part of multiple interlayers, to bond tungsten and steel. Yang et al. [107] looked into diffusion bonding between tungsten and 0Cr13Al ferritic stainless steel using a multilayer configuration. The schematics of this diffusion bonding and a metallographic image showing the structure are shown in Figure 4. The average strength of the bond was found to be 256 MPa and the bond survived up to 60 cycles of thermal shock when quenched to room temperature from 700 °C. The V/Cu composite barrier interlayer was explored by Cai et al. [108] for diffusion bonding between tungsten and 17Cr steel. Here, in the configuration of W-V-Cu-steel, the W/V interface had the highest amount of residual stress concentration and failure occurred predominantly in the tungsten substrate near this region. Corrugated deformation was observed in the V/Cu and Cu/Steel interface, which was attributed to the softer nature of copper compared to vanadium and steel and a low melting point of Cu (close to the joining temperature). Residual stress was minimized in this configuration, and it was hypothesized that, during the cooling period, vanadium would transfer the residual stress from tungsten and eventually Cu would relieve the residual stress through plastic deformation. A Cu interlayer has also been used in diffusion bonds between the W-Cu composite and stainless steel at 1150 °C for different holding times [109]. It was found that the elements from the steel side exhibit intergranular diffusion while penetrating the Cu interlayer. Intermediate bonding time (60 min) produced the best quality of bonding. A shorter holding time of 15 min was not effective because the diffusion of elements was not fully carried out, while a longer holding time of 90 min caused coarse grain formation in the solid solution zone. The effect of holding time on diffusion bond was also observed by Zhang et al. [110], where tungsten and 316 L stainless steel were bonded though hot isostatic pressing (HIP) using a Cu interlayer. The HIP process was conducted under a temperature of 1050 °C and a pressure of 150 MPa for a holding time ranging from 0.5 to 2 h. Tungsten had a penetration depth of 7 μm into Cu for a 2 h holding time. Both W/Cu and Cu/steel interfaces had higher hardness values due to solid solution formation. A copper interlayer was used by Sun et al. [111] in joining tungsten alloy and 304 stainless steel. Within the tungsten/copper interface, copper atoms diffuse into the tungsten lattice, distorting the tungsten lattice. Tensile strength in the interface was increased from this, which was reported to be 265 MPa, 58% higher than the tensile strength of the joint without the copper interlayer, which has a tensile strength of 168 MPa.

Table 2. Diffusion bonding between tungsten and steel with Cu interlayer from the literature.

Bonded Materials	Interlayer	Bonding Parameters	Mechanical Properties	Microstructural Properties	Ref.
W-0Cr13Al ferritic stainless steel	Cu/90W-10Ni powder/Ni multilayer	1150 °C + 5 MPa + 60 min, vac < 6×10^{-3} Pa	Average strength 256 MPa, survived 700 °C to room temperature thermal shock for 60 cycles		[107]
W with 17Cr-0.1C steel	V/Cu interlayer	1050 °C, 1 h, 10 MPa	Highest strength of the joint is 402 MPa	Successful bonding with no brittle intermetallic reported	[108]
W-Cu composite with stainless steel	Cu	1150 °C for 15 to 90 min		$W_{0.6}Cu_{0.4}$, $Cu_{3.8}Ni$, and $Fe_{0.946}Ni_{0.054}$ compounds form at the interface	[109]
W and 316L stainless steel	Cu	1050 °C, 0.5 to 2 h, 150 MPa	Max shear strength of the joint is 480 MPa (for 2 h), max hardness 10.2 GPa (W-Cu interface)	No brittle intermetallic reported, increased hardness observed within W/Cu and Cu/steel interface	[110]
W alloy with 304 stainless steel	Cu	900 °C, 2 h, 20 MPa	Tensile strength of joint is 265 MPa		[111]

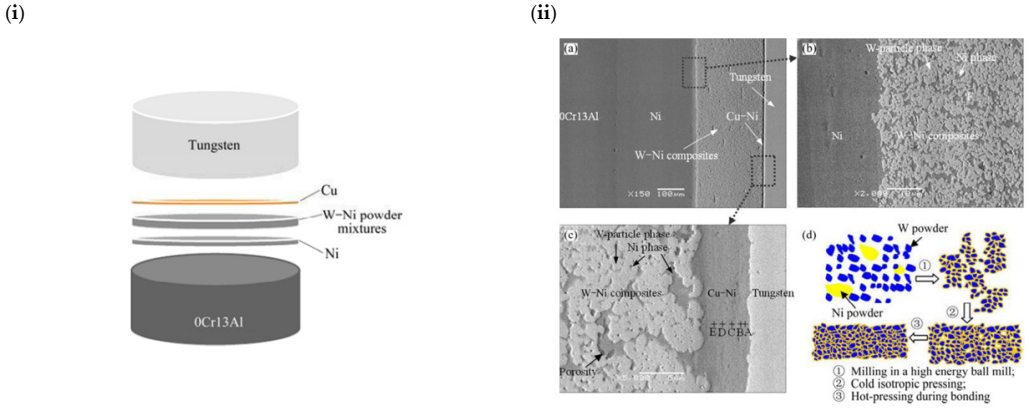


Figure 4. (**i**) Schematic of Tungsten-0Cr13Al steel diffusion bonding with Cu/W-Ni/Ni interlayer configuration; (**ii**) showing micrograph of interfaces where (**a**) shows the whole joint structure, (**b**) shows the interface Ni/W-Ni composite, (**c**) shows the W-Ni composites/Cu-Ni and Cu-Ni/tungsten, and (**d**) is a schematic drawing showing formation of W-Ni composites. Reprinted from reference [107], 2014, with permission from Elsevier.

Brazing with a copper interlayer is a possible approach for joining tungsten and steel. However, the brazing process involves the interlayer materials being melted to produce the bond [112]. In some cases where high temperature is used during brazing, recrystallization and grain growth can occur, especially on the steel side, which results in a weakened interface and inferior bonding [15,113].

Copper has a very high thermal conductivity [114] and the use of copper would be beneficial to remove heat. A phase diagram of Fe-W-Cu at 600 °C is shown in Figure 5. When Cu is joined with tungsten and steel, there is always going to be formation of undesirable phases like Laves phase and Fe_7W_6 (μ phase). While having a dispersed μ phase and Laves phase can enhance the high temperature performance of structural materials in some cases, the presence of these phases can also deteriorate the mechanical properties of the materials [115,116]. Even though a fully miscible region with a single phase structure is not possible to be produced in the W-Cu-Fe combination, the possibility remains to use Cu as an interlayer for joining tungsten and steel which can be used at high temperatures of up to 700 °C. This could open up new avenues to be explored in high temperature use in power plants, automobiles, etc. However, for the nuclear industry where irradiation is an issue, there may be strict limitations on elements and impurity related to copper for maintaining low activation so that, eventually, shallow burial is possible for nuclear waste after reactor decommission [100–102]. Therefore, a different low activation transition layer is necessary to produce a good transition bond between tungsten and steel while avoiding any brittle intermetallic [75].

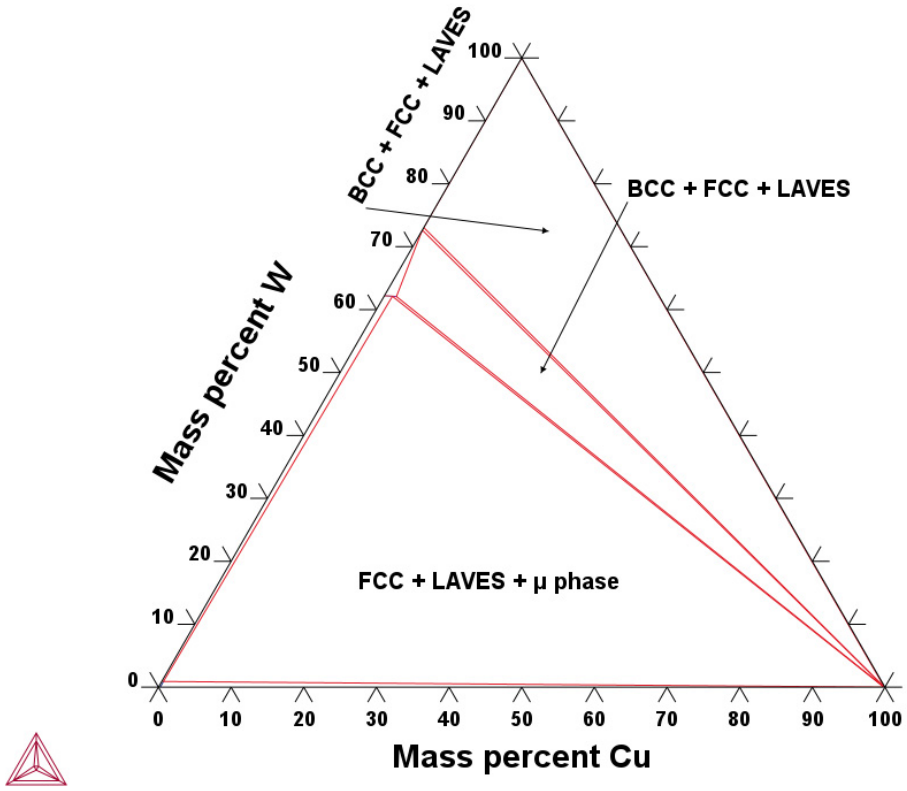


Figure 5. Fe-Cu-W ternary phase diagram at 600 °C calculated from TEFE9 database in Thermo-Calc.

5.2. Nickel Interlayer

In several studies, a nickel interlayer has been used as a single or part of multiple interlayers in joining tungsten and steel [117–120]. A summary of these studies is presented in Table 3. Zhong et al. [117] explored the effect of holding time on microstructural and mechanical properties for tungsten/ferritic steel joints with Ni interlayer diffusion bonded at 900 °C. According to the W-Ni binary phase diagram, it is possible to form intermetallic compounds such as Ni_4W, NiW, and NiW_2 [121]. However, according to Zhong et al., Ni_4W was formed only when the holding time was more than 1.5 h and no intermetallic was found below this time. A possible reason for no traceability of the other intermetallic phases could be due to the slow diffusion of W in Ni. Ni_4W has the lowest amount of W, which should form fastest among the intermetallic phases. Difficulties in the nucleation and growth were attributed to the absence of intermetallics. Intermetallic Ni_4W has a D1a ordering structure of the Ni_4Mo type (a = 5.733 Å, c = 3.554 Å) [122]. Another work of Zhong [28] focused on the effect of joining temperature on the properties of tungsten/steel joints with a Ni interlayer. A small amount of Ni_4W was formed with the holding temperature of 950 °C, but the strength of the joint was increased with the increase in the joining temperature up to 900 °C. No trace of intermetallic was found at the holding temperature of 850 °C and as a probable cause it was assumed that the incubation period for nucleating the intermetallic phase was very large or the holding time and/or temperature were not enough to cause the formation of intermetallic as dictated by the phase diagram of Ni-W. Feng et al. [118] studied diffusion bonding of functionally graded WC-Co/Ni (FGWC) and 410 stainless steel (410ss). The tensile strength of the joint increased at first and then decreased with the increase in holding temperature and time. A maximum tensile strength of 195 MPa was observed for a temperature of 950 °C and holding time of 80 min. Shorter or longer holding time resulted in lower strength; at a shorter time, there is insufficient diffusion, while a longer holding time causes grain growth. In another experiment, Liu et al. [119] used V/Ni composite interlayers in a W/steel diffusion-bonded joint (W-V-Ni-steel configuration) where the diffusion bonding was carried out in a vacuum at 1050 °C and 10 MPa for 1 h. The

schematics of the bonding configuration and the cross-section of the tungsten/steel-bonded joint with Ni and V interlayers are shown in Figure 6. Intermetallic Ni_3V, Ni_2V, Ni_2V_3, and NiV_3 were found in the Ni/V interface. Specimens fractured in a brittle mode within the tungsten substrate near the V/W interface during tensile tests. A Ti/Ni composite was used in the tungsten–steel joint (W-Ti-Ni-steel configuration) and the influence of the intermetallic phase on the microstructure and mechanical properties was analyzed [120]. No intermetallic was found in the W/Ti and Ni/steel interfaces but Ti_2Ni, TiNi, and $TiNi_3$ intermetallics were found in the Ti/Ni interface due to strong interaction between Ti and Ni. The joint fractured at the W/Ti interface at lower joining temperatures or short holding times. At higher joining temperatures and longer holding times, fracture occurs at the Ti/Ni interface in the intermetallic zone. The diffusion between electrodeposited Ni and 9Cr ferritic/martensitic steel was explored by Gao et al. [123]. The diffusion zone was found to be enriched with a solid solution of $\gamma_{Fe,Ni}$ rich in Ni. Tempering treatment was found to enhance the mechanical properties of the joint and fractures were found in the base steel during mechanical testing. A Nb/Ni composite interlayer has also been explored by Chen et al. [124] in the diffusion bonding between tungsten and MA956 steel (W-Nb-Ni-steel configuration). Ni_6Nb_7 and Ni_3Nb intermetallic were found in the Nb/Ni interfaces but the interfaces of the Ni/MA956 steel and W/Nb interface remained intermetallic-free. In shear experiments, the fractures occurred in the Nb/Ni interface, indicating the lower strength of this interface. In the work conducted by Wang et al. [125], the Ni-Si-B interlayer was used to join tungsten and steel through hot isostatic pressing. Here, the bonding steps were described by three different processes including solid–solid interaction, remaining interlayer liquefaction, and solid–liquid interaction. The influence of Si was found to be significant in the quality of the bond. The maximum bonding strength was reported to be 363.5 MPa. Wang et al. [126] used interlayer W-Cu-Ni to join tungsten and steel. The pressure during diffusion bonding varied from 10 to 20 MPa, while the temperature was kept at 1120 °C and the holding time was 60 min. An amount of 20 MPa pressure produced a better bonding with a bonding line width of 0.5 μm and shear strength 275 ± 12 MPa.

Table 3. Diffusion bonding between tungsten and steel with Ni interlayer from the literature.

Bonded Materials	Interlayer	Bonding Parameters	Mechanical Properties	Microstructural Properties	Ref.
W-ferritic steel	Ni	850 °C, 900 °C, 950 °C for 1.5 h	Max strength of joint is ~200 MPa at 900 °C	Solid solution-strengthened diffusion zone had increased hardness	[28]
W-ferritic steel	Ni	900 °C, 0.5 to 2 h	Avg. strength 215 MPa for 1 h holding time, max hardness 8.5 GPa	Interdiffusion layer increases with holding time	[117]
WC-Co/Ni composite with 410 stainless steel		1300 °C, 2 h, 5 KPa	Max tensile strength of joint is 195 MPa bonded at 950 °C for 80 min		[118]
W with 17Cr ferritic steel	V/Ni	1050 °C, 1 h, 10 MPa	Tensile strength 362 MPa	Ni_3V, Ni_2V, Ni_2V_3, and NiV_3 formed in the Ni/V interlayer	[119]
W with 19 Cr ferritic steel	Ti/Ni	850–1050 °C, 30–120 min, 10 MPa	Max tensile strength ~267 MPa	No intermetallic in W/Ti and Ni/Steel interface but Ti_2Ni, TiNi, and $TiNi_3$ formed at Ti/Ni interface	[120]
9Cr ferritic steels	Electrodeposited Ni	1050 °C, 1 h, 20 MPa	After tempering engineering stress ~460 MPa with ~37% elongation	FCC * structured $\gamma_{Fe,Ni}$ formed, no intermetallic	[123]
W with MA956 steel	Ni/Nb	1050 °C, 20 min, 20 MPa	Max shear strength 270 MPa, highest hardness 480 HV	Nb/Ni interface Ni_6Nb_7 and Ni_3Nb formed; fracture occurred in Nb/Ni interface on the Nb side	[124]

Table 3. *Cont.*

Bonded Materials	Interlayer	Bonding Parameters	Mechanical Properties	Microstructural Properties	Ref.
Tungsten with 304 stainless steel	Ni-Si-B	1020 °C, 2 h, 120 MPa	Maximum bonding strength 363.5 MPa		[125]
WC-Co-Ni and SS304 sintered together		Sintered at 1300 °C, for holding times of 30, 60, 90, and 120 min	Average maximum hardness is 1500 HV		[127]

* FCC = Face-centered cubic.

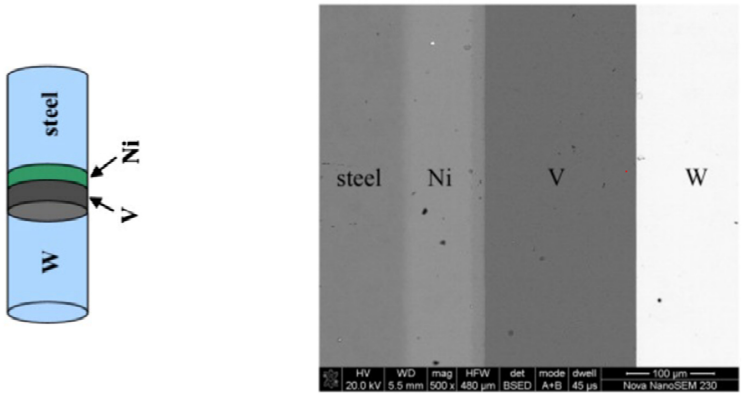


Figure 6. Scanning electron micrograph showing the schematics and cross-section of W/steel bond with insertion of Ni and V interlayers; reprinted from Ref. [119], 2013, with permission from Elsevier.

Nickel typically cannot be used as an in-vessel structural component in a fusion reactor due to several issues like very long half-life from neutron activation, neutron-induced void swelling, high helium (He) production, and associated embrittlement [100–102,128,129]. However, some nickel alloys are well known as high-temperature materials [130]. Ni has a face-centered cubic (FCC) crystal structure and based on the phase diagram presented in Figure 7, it is indicative that any elemental composition containing iron, tungsten, and nickel is going to produce intermetallic phases and a fully body-centered cubic (BCC) miscible zone is not possible. However, Ni is an essential element of austenitic stainless steel which has an FCC crystal structure and is known to possess good weldability, machinability, and excellent mechanical properties in high-temperature applications [131].

5.3. Titanium Interlayer

A summary of conducted studies where titanium was used as an interlayer while bonding tungsten and steel is presented in Table 4. Ti interlayers have recently gained significant attention as a potential solution for tungsten and steel bonding. Zhong et al. [132] performed diffusion bonding between tungsten and reduced-activation ferritic steel F82H, showing that all the interfaces were free from discontinuities and cracks. A scanning electron micrograph of the cross-section of this diffusion-bonded layer is shown in Figure 8. However, a few transverse cracks were found in the W/Ti interface, which was attributed to the enhanced interaction between W and Ti that caused cracking due to different atomic sizes of W and Ti. The W/Ti interface had three distinct regions including W and Ti: (1) W, (2) β-W-Ti solid solution with transformed α-Ti, and (3) α-Ti. W was found to diffuse further into the Ti side compared to Ti diffusion into the tungsten side; this is due to the higher diffusivity of W in Ti [133]. On the Ti/steel interface, the diffusion path was Ti/α-β Ti/stabilized α-β Ti/FeTi + Fe_2Ti+Cr_2Ti/α-Fe/F82H. During shear testing, all the joints fractured at the Ti/F82H interface. The pulsed plasma sintering (PPS) method was used to join W and steel with an interlayer of an Fe-Ti composite (25 wt% Fe + 75 wt% Ti and 86 wt% Fe + 14 wt% Ti). Fe_2Ti, TiC, and $Fe_{9.64}Ti_{0.36}$ phases were found in the W/86FeTi/EUROFER97 joint and α-Fe was found in the W/Fe/EUROFER97 joint [134]. Jung et al. [8] explored a HIP process to join tungsten and ferritic martensitic steel with

Ti interlayers. HIP was conducted in two steps, 900 °C with 100 MPa for 1.5 h and then 750 °C with 70 MPa for 2 h, where the first HIP step was for diffusion bonding of different interlayers and the second step was a tempering process of the steel. No diffusion layers were observed in the W/Ti interface, but a diffusion layer formed continuously in the Ti foil/steel interface. This diffusion layer was assumed to be consistent with FeTi, Fe_2Ti, and χ-phases ($Fe_{17}Cr_7Ti_5$). Chen et al. [135] investigated W/Fe diffusion bonding with Ti foil (Ti-f) and Ti powder (Ti-p) using spark plasma sintering (SPS). Ti-F was found to be more suitable as an interlayer compared to Ti-P. The bond using Ti-F was also found to be more thermally stable. Intermetallic FeTi was found in the Ti-F/Fe interface. Wang et al. [17] explored W/P91 steel with a Ti interlayer using HIP. Bonding in the Ti/W interface was limited due to residual stress concentration. Also, according to Hume-Rothery rules, elements with the same crystal structure will have appreciable solid solution [136]. Tungsten has a BCC crystal structure, and at 760 °C, Ti exhibits a hexagonal closed packed (HCP) structure (α-Ti). So, according to the Hume-Rothery rules, BCC-structured tungsten has limited diffusivity in HCP-structured titanium and, therefore, only a short diffusion distance was observed. However, note that beyond 880 °C, Ti has a BCC structure and, therefore, is fully soluble into tungsten. This means that for a diffusion bonding between tungsten and titanium performed at 880 °C or a composition where tungsten composition with titanium is kept below 10 wt%, it will produce a solid solution interface with BCC structure. Wang [17] also found a minimum shear strength of 225 MPa and fracture took place in the W/Ti interface. High hardness values in the interfaces are due to solid solution strengthening resulting from the atomic interdiffusion. Oxide dispersion-strengthened (ODS) steel was also considered by Noto [137] to bond with tungsten using a V-4Cr-4Ti interlayer. Ti was used in between ODS steel and V-4Cr-4Ti to inhibit the formation of the σ phase with the exception that low diffusivity of V in Ti would retard the migration of V into the steel side. Adjacent to the Ti layer, an Fe_2Ti compound formed, but with aging treatment, it was determined that Fe_2Ti does not have a detrimental effect on the bonding strength.

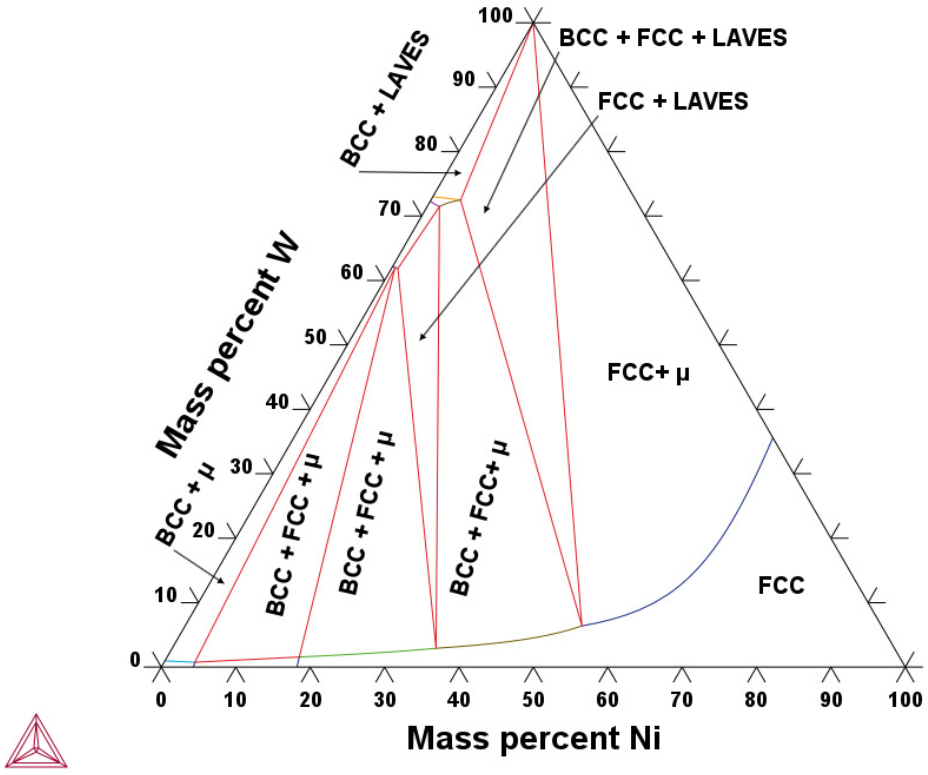


Figure 7. W-Ni-Fe phase diagram at 600 °C calculated from TEFE9 database in Thermo-Calc.

Table 4. Diffusion bonding between tungsten and steel with Ti interlayer from the literature.

Bonded Materials	Interlayer	Bonding Parameters	Mechanical Properties	Microstructural Properties	Ref.
W with F82H steel	Ti	850–950 °C, 1 h, 10 MPa	Max shear strength 113 MPa, highest hardness 6.8 GPa	Diffusion path: Ti/α-β Ti/stabilized β Ti/FeTi + Fe_2Ti + Cr_2Ti/α-Fe/F82H	[132]
W -EUROFER97	Two Fe-Ti thin layers	1000 °C, 10 min	Hardness of Ti samples was 240 Hv and hardness of Fe sample was 120 Hv	Phases such as Fe2Ti, TiC, and αFe9.64Ti0.36 were found in both W/86FeTi/Eurofer 97 joint and 86FeTi sinter	[134]
W with F82H steel	Ti	900 °C, 100 MPa, 1.5 h and 750 °C, 70 MPa, 2 h	Interface hardness 438–338 HV	Ti/F82H has a 200 μm interface	[8]
W and Fe	Ti foil and Ti powder	950 °C, 57 MPa, 5 min	Ti-Fe interface has a hardness of 266 HV	Typical microstructure of joining defects and pores, interdiffusion between W/Ti/Fe interface and the presence of solid solution	[135]
W with P91 steel	Ti	760 °C, 4 h	Min shear strength 225MPa, hardness 3.4 and 4.6 GPa for P91/Ti and Ti/W interface, respectively	Solid solution occurring through diffusion caused increased hardness in Ti/W interface	[17]
ODS steel with V-4Cr-4Ti	Ti	1250 °C, 10 MPa, 1 h	Fracture strength of 260 MPa before aging	Fe_2Ti form in Fe/Ti interface	[137]

From the binary phase diagram of Ti and Fe in Figure 9a, it is known that the solubility of Fe in HCP Ti is very limited (<0.1 at%) and FeTi and Fe_2Ti intermetallics form in the interface when Ti and Fe are joined together, which contribute to the embrittlement of the joint interface [138–143]. Particularly, FeTi is known to crack spontaneously when subjected to thermal stress [144]. Formation of $Ti_5Fe_7Cr_{15}$ was also reported in a welding joint of a Ti alloy and stainless steel [145]. Formation of the σ phase was also reported by Chatterjee [146] for pure Ti and an austenitic steel bond at 850–950 °C for 1 h. The σ phase exhibits a tetragonal structure [147] and it is well known for decreasing the toughness [148]. It should be noted that the σ phase also forms even without the Ti phase [149]. Moreover, from Figure 9b, where a 600 °C isotherm of W-Fe-Ti is shown, it is clear that a solid solution without the presence of intermetallic is impossible for the W-Fe-Ti system. However, even though Ti has very limited solid solubility within BCC Fe, there are other possible configurations where a BCC structure can be produced for an alloy system containing Ti. For example, such a phase diagram is shown in Figure 9c, where a V-Cr-Ti 600 °C isotherm is presented. The BCC marked area includes all the possible compositions of V, Cr, and Ti which can maintain a BCC structure at 600 °C. One such composition that produces a BCC structure can be integrated with tungsten and 9-Cr steel, both of which have a BCC zone at 600 °C. Research conducted by Gräning et al. [150] produced a transition structure between tungsten and steel where V-4Cr-4Ti was used as an interlayer in between tungsten and VCrAl to produce a smooth transition between tungsten and steel.

From a standpoint of neutron activation, Ti is a suitable element to be used in transition materials for fusion reactors [102], which makes it a potential candidate fusion reactor material [151]. However, some concerns remain due to tritium sequestration in Ti alloys resulting from high hydrogen solubility, and these should be taken into account for design considerations of fusion reactors [152].

5.4. Vanadium Interlayer

In Table 5, a few studies were summarized where vanadium was used as a single or a part of multiple interlayers while joining tungsten and steel. Vanadium can be a potential interlayer between tungsten and steel because of the high miscibility of V with W and Fe over a wide range of temperatures [18]. Basuki et al. [153] used V as an interlayer to join W with EUROFER97 reduced-activation ferritic steels through diffusion. A 4 μm brittle

σ phase was found at the steel/V interface and another carbide layer (presumably V_2C) of a thickness of 6 μm was also found on the V side near the same interface. The carbide layers exhibited a high hardness value peaking at 14 GPa. The Charpy impact energy of the joint was found to be relatively low (1.21 and 1.42 J/cm^2 for room temperature and at 550 °C, respectively); for comparison, high-carbon steel has a Charpy impact energy of 66 J/cm^2 [154]. Fracture occurred in the carbide formation region. At 1050 °C, recrystallization and grain coarsening occurred in the V interlayer. With the diffusion of V into steel, it was assumed that decarburization occurred in the steel structure because of the high affinity of carbon towards V, which results in a grain coarsening in the steel adjacent to the interface and could be observed up to 280 μm from the interface. Another work of Basuki [155] focused on the thermomechanical analysis of the W/EUROFER97 diffusion bond with a V interlayer which was subjected to thermal cycling between 350 and 500 °C under a constant tensile stress of 70 MPa. For a higher number of thermal cycles, the increase in interface region thickness was found to be negligible. However, the steel side lost its martensitic structure and grain growth was observed as the number of cycles was increased from 50 to 100 cycles. The Charpy impact energy for the interface was 2J, which is low compared to typical Charpy impact energies of steels. The mechanical behavior of the bonded sample was attributed to the combination of thin carbide layers, grain growth prevention, and sufficient closure of pores in the mating surface. The work of Basuki and Aktaa [156] focused on process optimization to reduce residual stress in the interfaces of W-V-EUFROFER97 diffusion bonding. Temperatures of 700 and 800 °C were used to reduce any kind of grain alteration of steel involving recrystallization and grain growth. It was found that the lower temperature reduced the residual stress in bond interfaces and limited the diffusion of carbon from the steel side to the V layer, which consequently lowered the thickness of the carbide layer. Superior ductility and impact toughness confirmed their hypothesis. However, lower temperature could limit the vacancy diffusion process and material transport is hindered in the interface, inhibiting the sintering of pores, especially at the W/V interface because of the low diffusivity of associated elements [157,158]. Increasing the bonding time from 1 h to 4 h seemed to improve the bonding while allowing a marginal growth of the carbide layer [156].

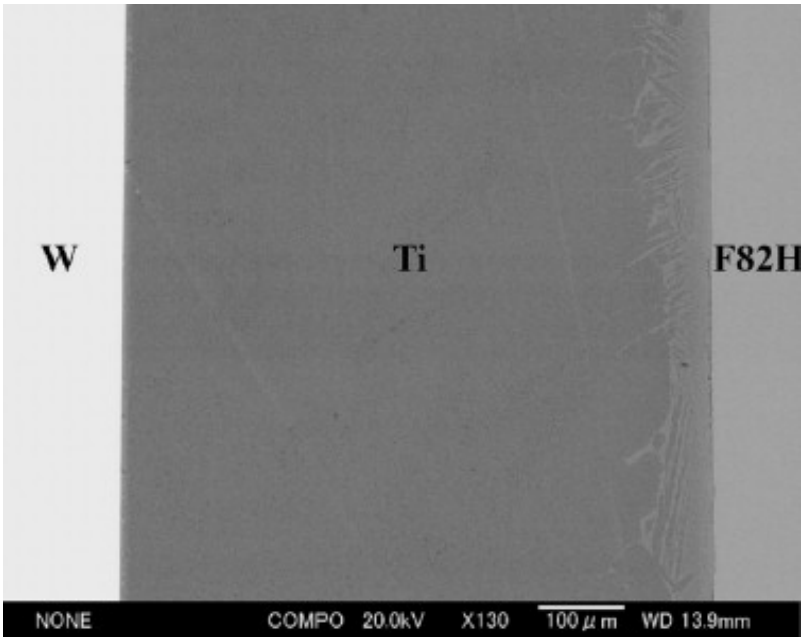
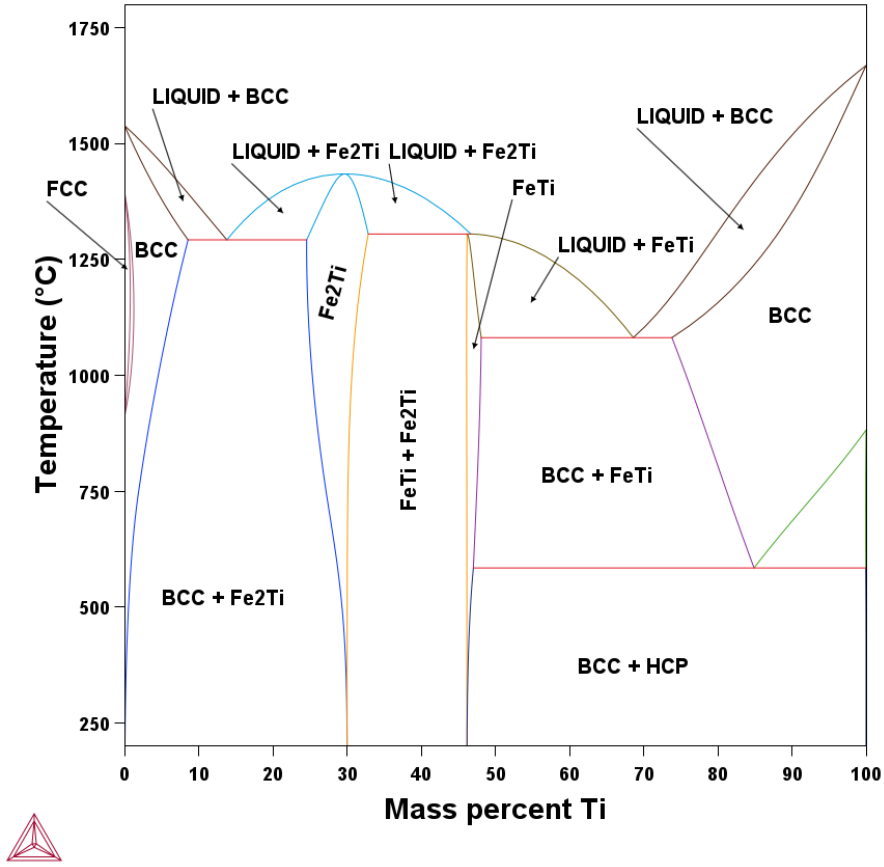
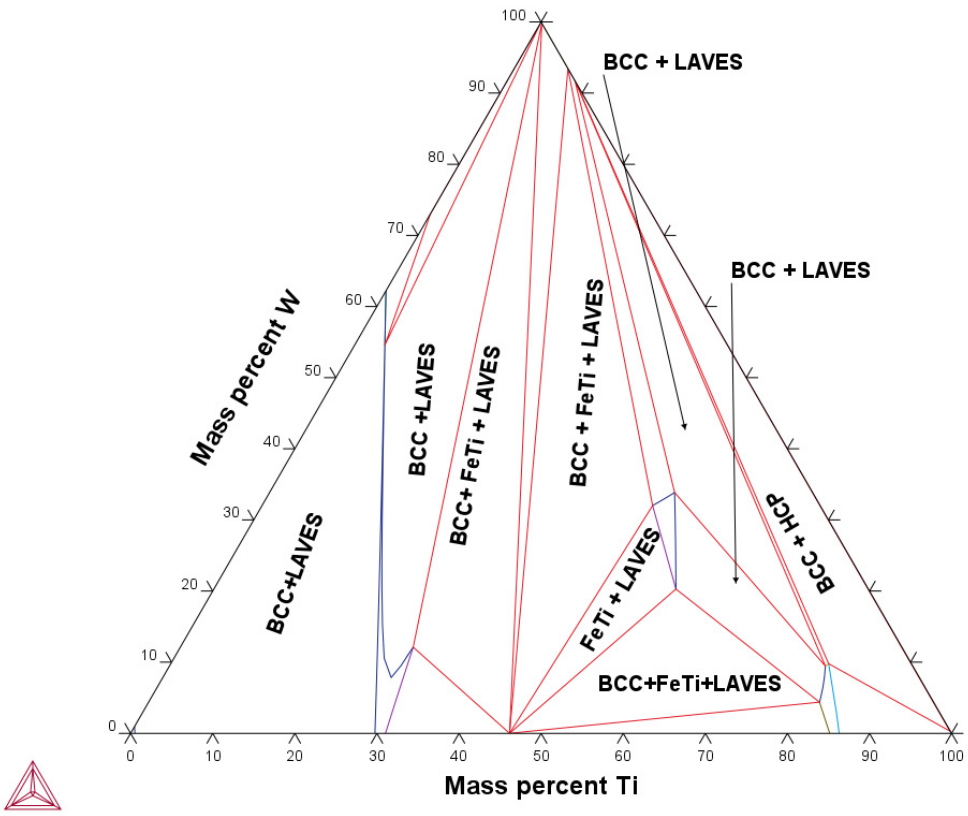


Figure 8. Scanning electron micrograph showing the cross-section of the diffusion-bonded tungsten and F82H steel with Ti interlayer annealed for 1 h. Reprinted from Ref. [132], 2010, with permission from Elsevier.

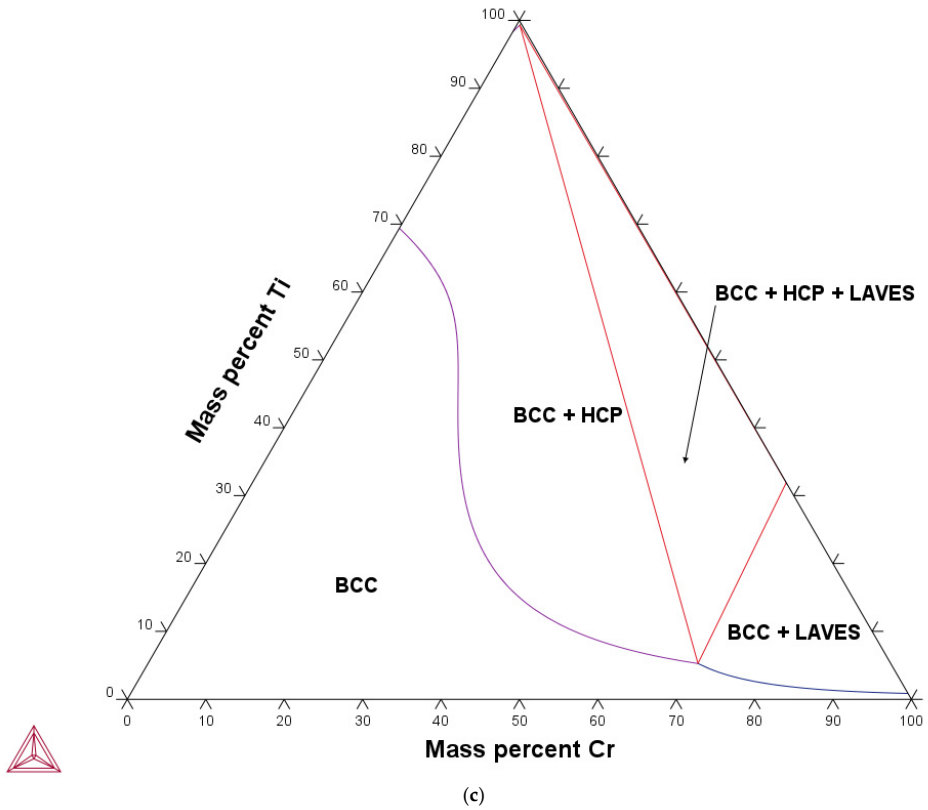


(a)



(b)

Figure 9. *Cont.*



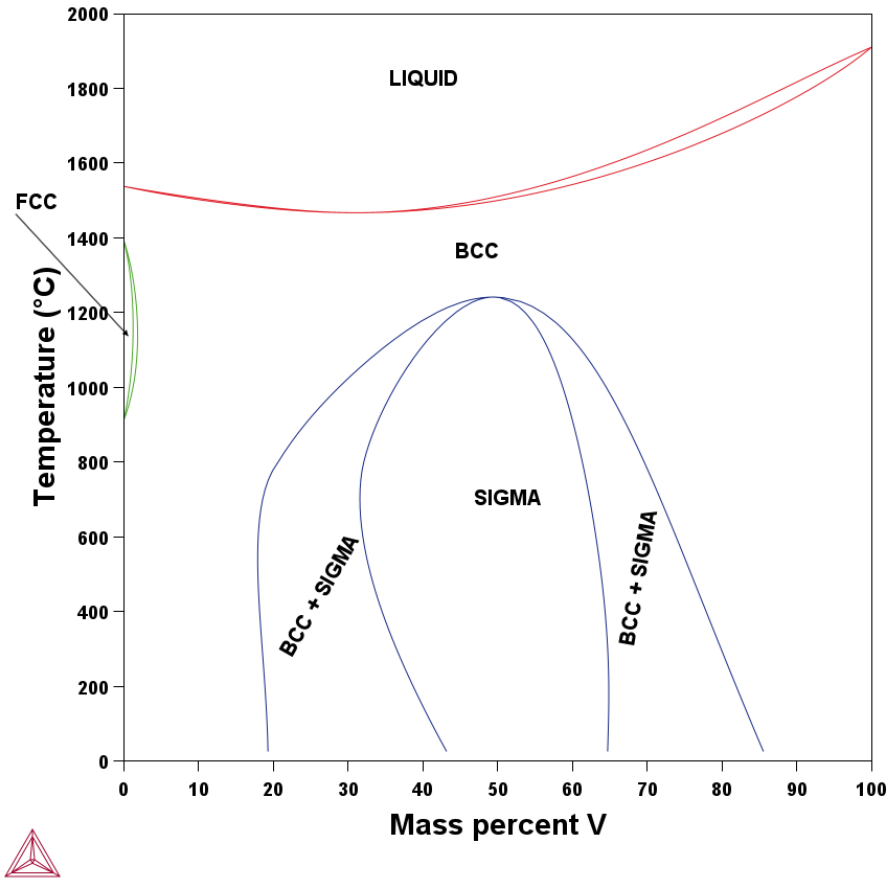
(**c**)

Figure 9. (**a**) Fe-Ti phase diagram calculated from TEFE9 database in Thermo-Calc. (**b**) Ternary phase diagram of W-Ti-Fe at 600 °C calculated from TEFE9 database in Thermo-Calc. (**c**) Ternary phase diagram of V-Cr-Ti at 600 °C calculated from TEFE9 database in Thermo-Calc.

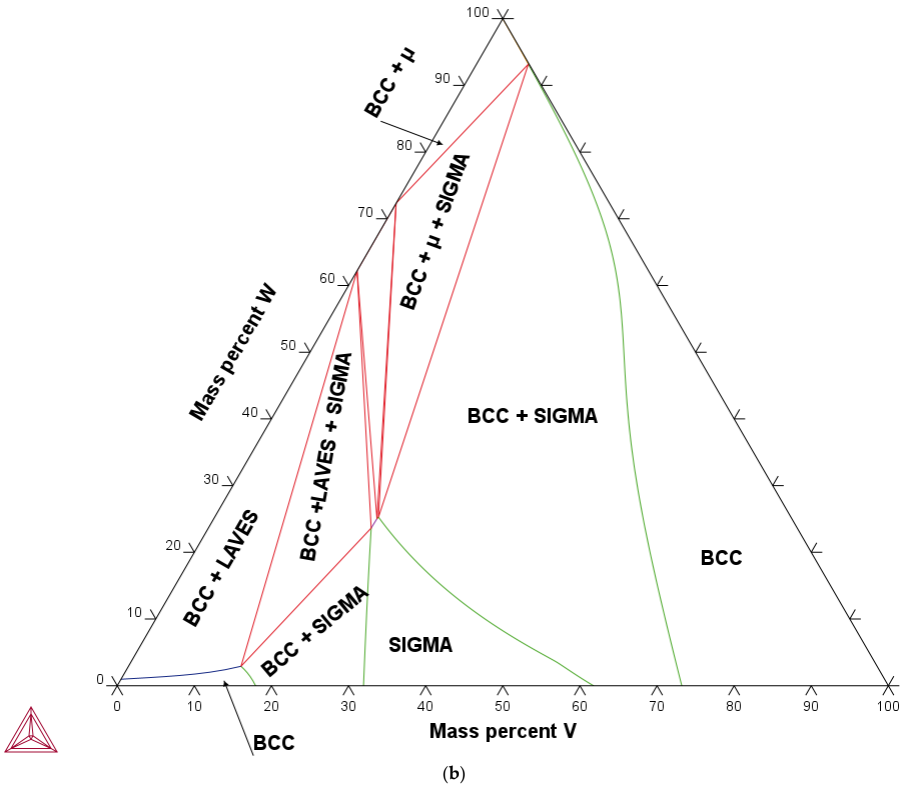
Table 5. Diffusion bonding between tungsten and steel with V interlayer from the literature.

Bonded Materials	Interlayer	Bonding Parameters	Mechanical Properties	Microstructural Properties	Ref.
W with 17Cr Ferritic steel	V/Ni	1050 °C, 1 h, 10 MPa	Tensile strength 362 Mpa	Ni_3V, Ni_2V, Ni_2V_3, and NiV_3 formed in the Ni/V interlayer	[119]
W-Eurofer97	V	1050 °C for 1, 3, and 4 h	RT joint property: UTS = 207 MPa, av = 1.21 J/cm^2,	Σ phase on steel side and V_2C on V side of the Fe/V interface	[153]
W-Eurofer97	V	T = 700 °C, 4 h, 10% creep strain rate on EUROFER97 side	YS = 324 MPa, Charpy Impact energy at 550 °C = 2.01 J	Thin VC layer formed, growth of α close to interface after 100 cycles	[155]
W-Eurofer97	V	700, 800, 1050 °C for 1 h, 700 °C for 4 h	291 MPa (550 °C) and 332 MPa (RT), elongation to fracture 20%, Charpy energy 2 J	Formation of VC, higher temperature reduces the thickness of VC	[156]

As it can be seen in Figure 10a, full miscibility exists between Fe and V when the V concentration is kept below ~18 wt%, while a fully BCC region exists in the W-V-Fe 600 °C isotherm as shown in Figure 10b [18]. Due to the high range of miscibility in the phase diagram, it is possible to choose a wide range of compositions including V as an interlayer between tungsten and steel. However, just one single layer of a V interlayer is not enough to reduce mechanical property gradient between tungsten and steel. This is because the difference in the coefficient of thermal expansion between tungsten and steel is very high and just one interlayer without any graded composition is simply not going to reduce enough of the mechanical property gradient to accommodate stress resulting from thermomechanical loads in service conditions. One possible approach could be to choose multiple layers of V-based alloys. This was shown by Gräning [150] where V-Cr-Ti and V-Cr-Al were used as two interlayers which maintained a fully BCC structure in a temperature range from 600 °C to 1150 °C



(**a**)



(**b**)

Figure 10. (**a**) V-Fe phase diagram calculated from TEFE9 database in Thermo-Calc. (**b**) W-V-Fe 600 °C isotherm ternary phase diagram calculated from TEFE9 database in Thermo-Calc.

V has been used as an element in steel because of the formation of V (C,N) precipitates which give rise to superior creep properties at high temperature [159]. V also shows a high-temperature strength and excellent thermal stress factor [160]. V is also a potential material for fusion reactors from an activation perspective and because of its favorable mechanical properties [102]. In a recent publication by Gräning [150], V-4Cr-4Ti was used as an interlayer in a novel W-steel transition design where a solid solution (without the presence of intermetallics) was reported. In terms of suitable transition materials, this is a very encouraging result.

5.5. Other Diffusion Bond Configurations

Elements like aluminum and niobium [161–163] have also been investigated as interlayers to join tungsten and steel. Basuki [161] reported the use of a Nb interlayer in a tungsten/EUROFER97 bond where intermetallic Nb_2C and Nb_6C_5 were observed and a relatively low room temperature impact energy of 1.5 J/cm^2 was reported. The use of Nb in fusion reactors is also prohibitive due to high activation [102]. In reduced-activation ferritic martensitic steel, Nb is replaced by Ta due to this high activation of Nb [20]. The hot isostatic pressing co-sintering method was used by Zhu et al. [164] where a tungsten alloy with a steel composite was fabricated. The tungsten interface was found to be the weakest link of the structure. Intermetallics found in this interface were η-carbides that contain Fe_3W_3C and Fe_6W_6C with thicknesses ranging from 4 to 6 μm and a Laves phase (Fe_2W). Another study where hot isostatic pressing was also used was performed by Liu et al. [165], where a 93W–4.9Ni–2.1Fe alloy and 30CrMnSiNi2A steel were bonded through diffusion. Intermetallic Fe_7W_6 was formed in the interface of the tungsten/steel zone. The reported average tensile strength was ~310.5 MPa and elongation was 8.6%. Another study with a fast sintering process to join functionally graded iron and tungsten was performed by Heuer et al. [166], where the synthesized tungsten/iron joint was subjected to temperatures of 300 °C, 500 °C, and 800 °C for up to 72 h. In all annealing conditions, the presence of Fe_7W_6 was reported. Composite interlayers have been used to produce hybrid bonding of tungsten/steel as reported by Yang et al. [167], where Ni from the composite interlayer agglomerated in the bonding zone and a shear strength of 263 ± 7 MPa was reported. High-entropy alloys have also been considered in different studies to be used as interlayers while joining tungsten and steel, like in [168], where a CrFeCoNiCu high-entropy alloy interlayer was used to bond tungsten alloy/steel through diffusion bonding, and [169], where an FeClCrNi high-entropy alloy was used for joining tungsten and China Low Activation Martensitic (CLAM) steel through vacuum diffusion bonding. Other interlayer like NiFeW [170] was also used to join tungsten to 30CrMnSiA steel. Self-passivating W-Cr-Y was joined with P91 steel by hot isostatic pressing, which was reported by Sal et al. [170]. Current-assisted sintered bonding was considered by Ganesh et al. [171], where a tungsten–steel joint was synthesized through plasma spraying to produce the graded structure. In the same study, current-assisted spark plasma sintering was also used to produce the graded W/V/75W/50W/25W/steel structure. The plasma spraying method yielded a very limited thermal conductivity that ranges between 15 and 25 Wm^{-1}K^{-1}. Some other numerical-based simulation studies were conducted while bonding tungsten and steel. Lu et al. [172] explored a tungsten–steel joint processed through hot isostatic pressing, where experimental investigations and first principle calculations were leveraged together to investigate the bonding interface. Crack initiation in the joint under loading conditions has been explored through the presence of intermetallics within the interface. On the other hand, numerical simulation was leveraged by Chen et al. [173] to explore resistant welded WC-10Co/B318 steel joints and the simulated result was complemented with the experimental values captured through a high-velocity camera. The major application for tungsten–steel joining is fusion reactor applications, and efforts from Grammes et al. [174] were dedicated to the exploration of tungsten and reduced-activation EUROFER steel joined through the vacuum plasma spraying method. This study was more focused on the design aspect and extensive microstructure and mechanical characterizations of

the interfaces were not conducted. However, in this research, a successful design of a cooling channel was implemented. Another research study focused on the design aspect of the graded tungsten–steel joining of the first wall in fusion reactors that is subjected to high heat flux [171]. Here, Ganesh et al. performed up to 200 thermal cycles and the plasma spraying tungsten–steel joint with a vanadium interlayer survived until 3 MW/m^2. Some other studies where bonding was established in a tungsten–steel configuration were conducted with additive manufacturing by Wei et al. [175] and friction stir welding by Khedr et al. [176]. Some other studies reported different configurations of bonding with either steel or tungsten but not both of them [38,44]. For example, a copper/steel dissimilar bond was reported by Chu et al. [177], where diffusion of Cu into steel resulted in severe cracking and the formation of Ni_2Si intermetallic was found. Friction stir welding was used by Joshani et al. [178] to produce a dissimilar joint of 7075 aluminum/AISI 304 stainless steel. Here, the formation of $FeAl_3$, Fe_3Si, FeAl, Fe_4Al_{13}, and $Fe_3Al_2Si_4$ intermetallics was reported. Two similar RAFM steels were used by Wei et al. [179], where both steels were joined through diffusion bonding with a temperature of 1050 C for 60 min and the pressure ranged from 10 to 20 MPa. Higher pressure produced a better bond and a more ductile fracture was reported, which is due to more disruption of oxide layers from the higher pressure. Some other studies have been conducted where the bonding between tungsten and steel was facilitated by a brazing process [177,180–185] and explosive diffusion bonding process [186]. From all these studies, valuable information regarding the diffusion characteristics of different combinations of elements can be acquired. This knowledge can be used to find a suitable configuration of interlayers for tungsten and steel that would produce a gradual mechanical property transition without forming brittle phases in the interfaces. It should be noted that formation of secondary phases or precipitates in a designed alloy system is often welcomed because high-temperature creep strength can be generated from appropriately dispersed high-density fine precipitates [187]. Problems arise when the secondary phases start to coarsen and delamination takes place in the interface of secondary phases and bulk phases due to stress concentrations, degrading the mechanical properties of the materials. Utilizing thermodynamic phase stability tools such as Thermo-Calc is valuable for designing an alloy system that can produce optimized mechanical and microstructural properties in the intended service conditions.

6. Discussion

The process of joining dissimilar materials holds significant importance across diverse industrial domains. Industries spanning the automotive, power, aerospace, transportation, and construction sectors necessitate the joining of different materials, including metals, steels, composites, polymers, thermoplastics, and so on [1,188–191]. Solid-state bonding offers a distinct advantage by facilitating the joining of dissimilar materials (particularly those with large differences in melting temperature) without causing degradation of their microstructure or mechanical properties resulting from very high temperature exposure and/or melting. This is made possible by circumventing the non-equilibrium transformations that are typically associated with the fusion welding process. Here, different configurations of tungsten and steel joining technologies were examined, utilizing a range of bonding techniques such as spark plasma sintering (SPS), hot press furnace, diffusion brazing, and plasma spraying. Apart from these techniques, some other solid-state bonding techniques such as linear and rotary friction welding, friction stir welding [192], ultrasonic welding [193], explosive welding [194], etc., are also available but have not been explored extensively for the joining of tungsten and steel.

All the different bonding techniques come with different advantages and disadvantages. For example, solid-state diffusion bonding with SPS can produce high joint strength when sufficient diffusion takes place between dissimilar materials, but it comes with the disadvantages of long processing time and a limited capability of producing complex shapes and structures [195]. Hot press furnace systems can produce uniform bonding with a homogeneous microstructure between dissimilar materials with the application

of uniform pressure, but they can be undesirable due to high equipment cost, limited bonding area, and extended processing time [196]. The unique advantage of the plasma spray bonding technique is the versatility, thickness control, enhanced wear resistance, thermal barrier properties, and superior bond strength, but porosity within bonding region, coating thickness variation, and higher cost should be taken into account when considering plasma spraying for the application of joining dissimilar materials [197]. On the other hand, diffusion brazing can also produce high-strength joints and is a relatively low-temperature process because of the typical lower melting temperature of filler materials, but thickness control is challenging due to the presence of sufficient filler materials and diffusion brazing comes with associated complexity because of the interaction between the filler and base materials [198].

Regarding diffusion bonding, the most important consideration is to establish atomic diffusion through the mating surfaces. A homologous temperature of >50% of the absolute melting temperature is necessary to induce sufficient atomic mobility for this diffusion [68]. In order to ensure a strong bond between tungsten and steel, considering their significant differences in mechanical properties and the tendency to form brittle intermetallic compounds, the incorporation of interlayers becomes crucial [199]. These interlayers play a vital role in minimizing the mechanical disparities and preventing the occurrence of embrittling phases during the bonding process [150]. For applications like fusion reactors that face severe thermomechanical loads, careful interlayer design is essential [200]. It involves creating suitable processing conditions to facilitate solid-state diffusion between the interlayers, reducing the mechanical property differences and avoiding the formation of brittle intermetallic compounds throughout the application's lifetime. Additionally, for high heat flux applications, the interlayers should possess sufficient thermal conductivity to minimize potential structural melting [201].

Based on the review that has been conducted in Section 5, the experimental data from different studies are very scattered and include a lot of different process parameters in different joining techniques as well as different compositions of interlayers between tungsten and steel. Several issues like the fracture of tungsten under pressure during joining or the formation of brittle intermetallic and potential solutions to avoid these issues were not scientifically explored. Further study on the fracture toughness in tungsten and the formation of brittle intermetallic in the joint are of paramount importance, because these factors can reduce the lifetime of structural materials significantly [202]. Furthermore, the composition and configuration of the tungsten–steel joint, with or without interlayers, were not formulated precisely using an accurate thermodynamic basis.

To ensure a successful bond and maintain the desired mechanical strength, durability, and thermal stability required for demanding applications, careful consideration should be given to the number of interlayers used. In light of the substantial differences in mechanical properties between tungsten and steel, it has been suggested, based on the work of Gräning [150], that using three interlayers could be an appropriate approach. This study employed a dissimilar materials joining configuration involving W-VCrTi-VCrAl-FeCrAl reduced-activation ferritic/martensitic steel. An image of this cross-section configuration is shown in Figure 11. Through careful thermodynamic calculations, a fully body-centered cubic (BCC) structure was achieved across the entire structure without the formation of intermetallic compounds, for the temperature range of 1100 °C to 650 °C. This number of interlayers helps minimize the mechanical property disparities while satisfying all the above mentioned criteria, which are (i) the minimization of the difference in the coefficients of thermal expansion, (ii) the elimination of the formation of brittle intermetallics, and (iii) ensuring sufficient diffusion between layers to form a sound bond that can withstand load expected in service conditions.

In the exploration of diffusion bonding, it is crucial to consider the fundamentals of materials science. The design of the bonding process should align with the specific requirements of the real-life application. For instance, if the application does not involve neutron irradiation, interlayer configurations consisting of elements with longer half-lives

can be considered. When selecting the materials to be joined, compatibility factors such as crystal structure, lattice parameters, coefficient of thermal expansion, and chemical activity should be taken into account. The interface reaction between interlayers is also a critical consideration, as the nucleation of secondary phases at the interface can lead to smaller grain boundaries, potentially compromising high-temperature creep strength. Adequate surface cleaning is vital to prevent the presence of impurities, which result in weak bonds and negatively impact the mechanical properties. Careful selection of bonding parameters, including temperature, time, and pressure, is essential to achieve proper diffusion bonding while avoiding recrystallization and grain growth that could adversely affect mechanical properties. Additionally, attention should be given to the heating and cooling rates to minimize any undesired non-equilibrium phase changes.

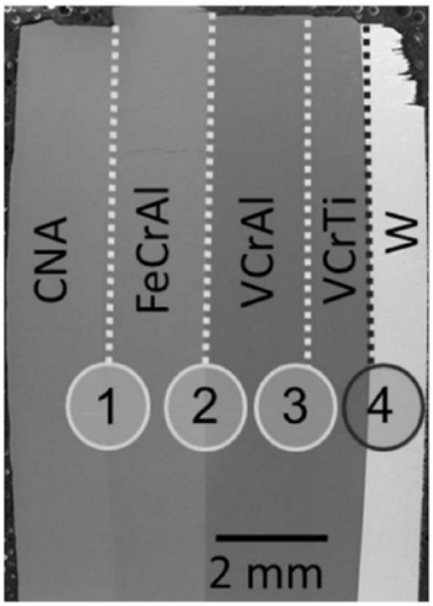


Figure 11. Cross-sectional view of tungsten steel transition layer with the insertion of VCrTi, VCrAl, and FeCrAl interlayers, producing a total of four interfaces marked as 1, 2, 4 and 4. Reprinted from Ref. [150], 2023, with permission from Elsevier.

In an industrial application, for example, aerospace, heat exchangers, automobiles, power plants, etc., the joining technique has to be capable of producing high-performance joints with acceptably short manufacturing time. This can be facilitated by the use of thermodynamics and numerical modeling which can predict the onset of temperature-induced defects, evolution of porosities, variation of phases and crystallinity, and even thermal degradation of the joining surfaces [191]. The post-bonding joint has to undergo comprehensive characterization under different temperatures to determine the time- and temperature-dependent microstructural and mechanical properties. A robust design based on process simulation tools would greatly advance the understanding of the joining technique and promote the development and optimization of the existing process [189,203]. There is a constant hunt for materials with high strength, robustness, performance, productivity, and sustainability. The development of novel processes or optimization of existing processes for joining materials can contribute to the identification and maturation of such high-performance materials. An increased understanding of basic bonding mechanisms is necessary for this and more extensive studies need to be performed for a comprehensive understanding of existing techniques. Furthermore, it is also imperative to devise new testing methodologies to effectively evaluate the basic bonding properties and quality of both new and existing technologies [1,42].

Acquiring comprehensive knowledge of failure mechanisms is crucial in the design stage to prevent structural failures. This can be achieved through a combination of ad-

vanced microscopy, microstructural characterization and mechanical testing, and numerical modeling. Typically, thermal expansion mismatches, residual stress, etc., cause failure during the short-term design phase. Formability gradients, bonding mechanisms, and heat capacity differences are responsible for failure during the processing phase. Thermal and mechanical load, corrosion, and phase changes due to aging cause failure during service conditions [1]. For failure analysis, an important advancement can be achieved through sensor-based monitoring and automated joint quality inspection. Combining all the knowledge on different aspects of pre- and post-joining stages will facilitate standardization of a joining technique, which is currently missing. There are no universally acknowledged benchmarks in place for solid-state bonding techniques. While individual industries have enhanced their internal process specifications, these refined measures remain inaccessible for public employment [191].

7. Conclusions

The key findings and future work from the review paper are listed below:

i Using the CALPHAD approach, this review paper evaluated the joining between tungsten and steel for direct bonding and bonding with an interlayer (titanium, copper, nickel, vanadium, niobium, etc.) for fusion reactor applications.

ii One recurring observation regarding the suitability of prospective interlayer configurations is their propensity to form brittle intermetallic phases at the joining interface, which can generally be linked to degradation of mechanical properties of the joint. To tailor the diffusion bond process, it is recommended to determine interlayer composition and configuration through thermodynamic calculations to prevent embrittling phases and minimize property gradients.

iii Variations in process parameters, surface treatments, and specimen geometry among different studies present challenges in objectively comparing results. Moreover, limited availability of mechanical testing data on bonded interfaces hinders drawing firm conclusions on the most promising interlayer approaches. Biases in reporting, heterogeneity in study designs, and limited validation and reproducibility impact the overall reliability and applicability of the research. To address these limitations, researchers should acknowledge the implications and promote data sharing, use standardized protocols, and conduct rigorous statistical analyses to enhance credibility and relevance in real-world scenarios.

iv The thermodynamic-based approach for solid-state bonding design between tungsten and steel is applicable beyond the nuclear field, extending to industries with extreme environments like high-temperature stress. This review paper's approach may guide future researchers in addressing challenges when joining dissimilar materials for practical engineering applications.

Author Contributions: Conceptualization: I.K.R.; methodology: I.K.R. and S.B.H.; data curation: I.K.R. and S.B.H.; writing—original draft preparation: I.K.R.; writing—review and editing: I.K.R., S.B.H., T.G., Y.Y., E.A.L. and S.J.Z.; supervision: T.G., Y.Y., E.A.L., Y.K. and S.J.Z.; funding acquisition: Y.K. and S.J.Z. All authors have read and agreed to the published version of the manuscript.

Funding: Support for the conducted research is provided by the U.S. Department of Energy (DOE), Advanced Research Projects Agency–Energy (ARPA-E) under Award Number 20/CJ000/08/03 at Oak Ridge National Laboratory and the Fusion Energy Science program.

Data Availability Statement: Data for this study are unavailable.

Conflicts of Interest: The authors declare that they have no known competing financial interests or personal relationships that could have appeared to influence the work reported in this paper.

References

1. Martinsen, K.; Hu, S.J.; Carlson, B.E. Joining of Dissimilar Materials. *CIRP Ann.* **2015**, *64*, 679–699. [CrossRef]
2. Wuli, C.P. The International Thermonuclear Experimental Reactor and the Future of Nuclear Fusion Energy. *Plasma Phys. Fusion Technol.* **2010**, *39*, 375–378.
3. Suri, A.; Krishnamurthy, N.; Batra, I. Materials Issues in Fusion Reactors. *J. Phys. Conf. Ser.* **2010**, *208*, 012001. [CrossRef]
4. Schumacher, U. Status and Problems of Fusion Reactor Development. *Naturwissenschaften* **2001**, *88*, 102–112. [CrossRef] [PubMed]
5. Zinkle, S.J.; Blanchard, J.P.; Callis, R.W.; Kessel, C.E.; Kurtz, R.J.; Lee, P.J.; McCarthy, K.A.; Morley, N.B.; Najmabadi, F.; Nygren, R.E.; et al. Fusion Materials Science and Technology Research Opportunities Now and during the ITER Era. *Fusion Eng. Des.* **2014**, *89*, 1579–1585. [CrossRef]
6. Pintsuk, G.; Aiello, G.; Dudarev, S.L.; Gorley, M.; Henry, J.; Richou, M.; Rieth, M.; Terentyev, D.; Vila, R. Materials for In-Vessel Components. *Fusion Eng. Des.* **2022**, *174*, 112994. [CrossRef]
7. Wirtz, M.; Uytdenhouwen, I.; Barabash, V.; Escourbiac, F.; Hirai, T.; Linke, J.; Loewenhoff, T.; Panayotis, S.; Pintsuk, G. Material Properties and Their Influence on the Behaviour of Tungsten as Plasma Facing Material. *Nucl. Fusion* **2017**, *57*, 066018. [CrossRef]
8. Jung, Y.I.; Park, J.Y.; Choi, B.K.; Lee, D.W.; Cho, S. Interfacial Microstructures of HIP Joined W and Ferritic–Martensitic Steel with Ti Interlayers. *Fusion Eng. Des.* **2013**, *88*, 2457–2460. [CrossRef]
9. Philipps, V. Tungsten as Material for Plasma-Facing Components in Fusion Devices. *J. Nucl. Mater.* **2011**, *415*, S2–S9. [CrossRef]
10. Coenen, J.; Antusch, S.; Aumann, M.; Biel, W.; Du, J. Materials for DEMO and Reactor Applications—Boundary Conditions and New Concepts. *Phys. Scr.* **2016**. [CrossRef]
11. Yin, C.; Terentyev, D.; Zhang, T.; Nogami, S.; Antusch, S.; Chang, C.C.; Petrov, R.H.; Pardoen, T. Ductile to Brittle Transition Temperature of Advanced Tungsten Alloys for Nuclear Fusion Applications Deduced by Miniaturized Three-Point Bending Tests. *Int. J. Refract. Met. Hard Mater.* **2021**, *95*, 105464. [CrossRef]
12. Farrell, K.; Schaffhauser, A.C.; Stiegler, J.O. Recrystallization, Grain Growth and the Ductile-Brittle Transition in Tungsten Sheet. *J. Less Common Met.* **1967**, *13*, 141–155. [CrossRef]
13. Tsuchida, K.; Miyazawa, T.; Hasegawa, A.; Nogami, S.; Fukuda, M. Recrystallization Behavior of Hot-Rolled Pure Tungsten and Its Alloy Plates during High-Temperature Annealing. *Nucl. Mater. Energy* **2018**, *15*, 158–163. [CrossRef]
14. Klueh, R.L.; Nelson, A.T. Ferritic/Martensitic Steels for next-Generation Reactors. *J. Nucl. Mater.* **2007**, *371*, 37–52. [CrossRef]
15. Bachurina, D.; Suchkov, A.; Filimonov, A.; Fedotov, I.; Savelyev, M.; Sevryukov, O.; Kalin, B. High-Temperature Brazing of Tungsten with Steel by Cu-Based Ribbon Brazing Alloys for DEMO. *Fusion Eng. Des.* **2019**, *146*, 1343–1346. [CrossRef]
16. Sun, L.; Song, X.; Dong, Y.; Zou, J.; Li, X.; Ni, L.; Gao, L.; Liang, S. Microstructure and Strength of Diffusion Bonded 304 Stainless Steel/Tungsten Joints Using Different Interlayers. *J. Manuf. Process.* **2021**, *65*, 428–434. [CrossRef]
17. Wang, J.C.; Wang, W.; Sun, Z.; Wang, X.; Wei, R.; Xie, C.; Li, Q.; Luo, G. nan Microstructure and Mechanical Analysis of W/P91 Steel HIP-Joint with Ti Interlayer. *Fusion Eng. Des.* **2016**, *112*, 67–73. [CrossRef]
18. Massalski, T.; Okamoto, H.; Subramanian, P. *Binary Alloy Phase Diagrams*; ASM International: Detroit, MI, USA, 1986.
19. Heuer, S.; Weber, T.; Pintsuk, G.; Coenen, J.W.; Matejicek, J.; Linsmeier, C. Aiming at Understanding Thermo-Mechanical Loads in the First Wall of DEMO: Stress–Strain Evolution in a Eurofer-Tungsten Test Component Featuring a Functionally Graded Interlayer. *Fusion Eng. Des.* **2018**, *135*. [CrossRef]
20. Tavassoli, A.A.F.; Alamo, A.; Bedel, L.; Forest, L.; Gentzbittel, J.M.; Rensman, J.W.; Diegele, E.; Lindau, R.; Schirra, M.; Schmitt, R.; et al. Materials Design Data for Reduced Activation Martensitic Steel Type EUROFER. *J. Nucl. Mater.* **2004**, *329*, 257–262. [CrossRef]
21. Gustafson, P. A Thermodynamic Evaluation of the C-Fe-W System. *Metall. Trans. A* **1987**, *18*, 175–188. [CrossRef]
22. Kattner, U.R.; Campbell, C.E. Invited Review: Modelling of Thermodynamics and Diffusion in Multicomponent Systems. *Mater. Sci. Technol.* **2013**, *25*, 443–459. [CrossRef]
23. Isomäki, I.; Hämäläinen, M.; Braga, M.H.; Gasik, M. First Principles, Thermal Stability and Thermodynamic Assessment of the Binary Ni-W System. *Int. J. Mater. Res.* **2017**, *108*, 1025–1035. [CrossRef]
24. Ojha, R.; Helander, T.; Kumar, K.C.H. Experimental Determination of Phase Equilibria in Fe-Cr-Ni-Al System. *J. Phase Equilibria Diffus.* **2021**, *42*, 428–438. [CrossRef]
25. Predel, F. *Phase Equilibria, Crystallographic and Thermodynamic Data of Binary Alloys*; Springer: Berlin/Heidelberg, Germany, 2016.
26. Dunkerton, S.B. Diffusion Bonding—An Overview. In *Diffusion Bonding 2*; Springer: Dordrecht, The Netherlands, 1991; pp. 1–12. [CrossRef]
27. Derby, B.; Wallach, E.R. Theoretical Model for Diffusion Bonding. Ph.D. Thesis, University of Cambridge, Cambridge, UK, 1998.
28. Zhong, Z.; Jung, H.C.; Hinoki, T.; Kohyama, A. Effect of Joining Temperature on the Microstructure and Strength of Tungsten/Ferritic Steel Joints Diffusion Bonded with a Nickel Interlayer. *J. Mater. Process. Technol.* **2010**, *210*, 1805–1810. [CrossRef]
29. AlHazaa, A.; Haneklaus, N.; Metals, Z.A. Impulse Pressure-Assisted Diffusion Bonding (IPADB): Review and Outlook. *Metals* **2021**, *11*, 323. [CrossRef]
30. Ismail, A.; Hussain, P.; Mustapha, M.; Nuruddin, F.; Saat, A.M.; Abdullah, A.; Aziz, A.; Rahim, A.; Chevalier, S. Fe-Al Diffusion Bonding: Effect of Reaction Time on the Interlayer Thickness. *J. Mech. Eng.* **2018**, *5*, 80–91.
31. Zuruzi, A.S.; Li, H.; Dong, G. Effects of Surface Roughness on the Diffusion Bonding of Al Alloy 6061 in Air. *Mater. Sci. Eng. A* **1999**, *270*, 244–248. [CrossRef]

32. Norrish, J. An Introduction to Welding Processes. In *Advanced Welding Processes*; Woodhead Publishing: Sawston, UK, 2006; pp. 1–15. ISBN 978-1-84569-130-1.
33. Selcuk Dr, C. Joining Processes for Powder Metallurgy Parts. *Adv. Powder Metall. Prop. Process. Appl.* **2013**, 380–398. [CrossRef]
34. Banerjee, S.; Mukhopadhyay, P. Diffusional Transformations. *Pergamon Mater. Ser.* **2007**, *12*, 555–716. [CrossRef]
35. Kazakov, N.F. An Outline of Diffusion Bonding in Vacuum. In *Diffusion Bonding of Materials*; Pergamon: Oxford, UK, 1985; pp. 10–16.
36. Shirzadi, A.A.; Assadi, H.; Wallach, E.R. Interface Evolution and Bond Strength When Diffusion Bonding Materials with Stable Oxide Films. *Surf. Interface Anal.* **2001**, *31*, 609–618. [CrossRef]
37. Shirzadi, A.A. Diffusion Bonding Aluminium Alloys and Composites: New Approaches and Modelling. Ph.D. Thesis, University of Cambridge, Cambridge, UK, 1997.
38. Mo, D.F.; Song, T.F.; Fang, Y.J.; Jiang, X.S.; Luo, C.Q.; Simpson, M.D.; Luo, Z.P. A Review on Diffusion Bonding between Titanium Alloys and Stainless Steels. *Adv. Mater. Sci. Eng.* **2018**, *2018*, 8701890. [CrossRef]
39. Metroke, T.L.; Parkhill, R.L.; Knobbe, E.T. Passivation of Metal Alloys Using Sol–Gel-Derived Materials—A Review. *Prog. Org. Coatings* **2001**, *41*, 233–238. [CrossRef]
40. Ohmi, T.; Ohki, A.; Nakamura, M.; Kawada, K.; Watanabe, T.; Nakagawa, Y.; Miyoshi, S.; Takahashi, S.; Chen, M.S.K. The Technology of Chromium Oxide Passivation on Stainless Steel Surface. *J. Electrochem. Soc.* **1993**, *140*, 1691–1699. [CrossRef]
41. Song, G.; Li, T.; Yu, J.; Liu, L. A Review of Bonding Immiscible Mg/Steel Dissimilar Metals. *Materials* **2018**, *11*, 2515. [CrossRef] [PubMed]
42. Carlone, P.; Astarita, A. Dissimilar Metal Welding. *Metals* **2019**, *9*, 1206. [CrossRef]
43. Kah, P.; Jukka Martikainen, M.S. Trends in Joining Dissimilar Metals by Welding. *Appl. Mech. Mater.* **2013**, *440*, 269–276. [CrossRef]
44. AlHazaa, A.; Metals, N.H. Diffusion Bonding and Transient Liquid Phase (TLP) Bonding of Type 304 and 316 Austenitic Stainless Steel—A Review of Similar and Dissimilar Material Joints. *Metals* **2020**, *10*, 613. [CrossRef]
45. Dunford, D.V.; Wisbey, A. Diffusion Bonding of Advanced Aerospace Metallics. *MRS Online Proc. Libr.* **1993**, *314*, 39–50. [CrossRef]
46. Lee, H.-S. Diffusion Bonding of Metal Alloys in Aerospace and Other Applications. *Weld. Join. Aerosp. Mater.* **2012**, 320–344. [CrossRef]
47. Campbell, F.C., Jr. *Manufacturing Technology for Aerospace Structural Materials*; Elsevier: Amsterdam, The Netherlands, 2011.
48. Lee, H.S.; Yoon, J.H.; Yoo, J.T. Manufacturing of Aerospace Parts with Diffusion Bonding Technology. *Appl. Mech. Mater.* **2011**, *87*, 182–185. [CrossRef]
49. Simões, S. Diffusion Bonding and Brazing of Advanced Materials. *Metals* **2018**, *8*, 959. [CrossRef]
50. Rowcliffe, A.F.; Zinkle, S.J.; Stubbins, J.F.; Edwards, D.J.; Alexander, D.J. Austenitic Stainless Steels and High Strength Copper Alloys for Fusion Components. *J. Nucl. Mater.* **1998**, *258–263*, 183–192. [CrossRef]
51. Ivanov, A.D.; Sato, S.; Le Marois, G. Evaluation of Hot Isostatic Pressing for Joining of Fusion Reactor Structural Components. *J. Nucl. Mater.* **2000**, *283–287*, 35–42. [CrossRef]
52. Odegard, B.C.; Kalin, B.A. A Review of the Joining Techniques for Plasma Facing Components in Fusion Reactors. *J. Nucl. Mater.* **1996**, *233–237*, 44–50. [CrossRef]
53. Odegard, B.C.; Cadden, C.H.; Watson, R.D.; Slattery, K.T. A Review of the US Joining Technologies for Plasma Facing Components in the ITER Fusion Reactor. *J. Nucl. Mater.* **1998**, *258–263*, 329–334. [CrossRef]
54. Chen, Y.; Huang, Y.; Li, F.; Han, L.; Liu, D.; Luo, L.; Ma, Z.; Liu, Y.; Wang, Z. High-Strength Diffusion Bonding of Oxide-Dispersion-Strengthened Tungsten and CuCrZr Alloy through Surface Nano-Activation and Cu Plating. *J. Mater. Sci. Technol.* **2021**, *92*, 186–194. [CrossRef]
55. Shin, J.H.; Yoon, S.H. Thermal and Hydraulic Performance of a Printed Circuit Heat Exchanger Using Two-Phase Nitrogen. *Appl. Therm. Eng.* **2020**, *168*, 114802. [CrossRef]
56. Li, Q.; Flamant, G.; Yuan, X.; Neveu, P.; Luo, L. Compact Heat Exchangers: A Review and Future Applications for a New Generation of High Temperature Solar Receivers. *Renew. Sustain. Energy Rev.* **2011**, *15*, 4855–4875. [CrossRef]
57. Pra, F.; Tochon, P.; Mauget, C.; Fokkens, J.; Willemsen, S. Promising Designs of Compact Heat Exchangers for Modular HTRs Using the Brayton Cycle. *Nucl. Eng. Des.* **2008**, *238*, 3160–3173. [CrossRef]
58. Wilden, J.; Jahn, S.; Beck, W. Some Examples of Current Diffusion Bonding Applications. *Materwiss. Werksttech.* **2008**, *39*, 349–352. [CrossRef]
59. Mylavarapu, S.K.; Sun, X.; Christensen, R.N.; Unocic, R.R.; Glosup, R.E.; Patterson, M.W. Fabrication and Design Aspects of High-Temperature Compact Diffusion Bonded Heat Exchangers. *Nucl. Eng. Des.* **2012**, *249*, 49–56. [CrossRef]
60. Chai, L.; Tassou, S.A. A Review of Printed Circuit Heat Exchangers for Helium and Supercritical CO2 Brayton Cycles. *Therm. Sci. Eng. Prog.* **2020**, *18*, 100543. [CrossRef]
61. Brandner, J.J.; Anurjew, E.; Bohn, L.; Hansjosten, E.; Henning, T.; Schygulla, U.; Wenka, A.; Schubert, K. Concepts and Realization of Microstructure Heat Exchangers for Enhanced Heat Transfer. *Exp. Therm. Fluid Sci.* **2006**, *30*, 801–809. [CrossRef]
62. Sabharwall, P.; Clark, D.; Glazoff, M.; Zheng, G.; Sridharan, K.; Anderson, M. Advanced Heat Exchanger Development for Molten Salts. *Nucl. Eng. Des.* **2014**, *280*, 42–56. [CrossRef]
63. Gietzelt, T.; Toth, V.; Technologies, A.H. *Diffusion Bonding: Influence of Process Parameters and Material Microstructure;Joining Technologies*; Intech Open Publishers: London, UK, 2016.

64. Assari, A.H.; Beitallah, E. Microstructure and Kinetics of Intermetallic Phase Formation during Solid State Diffusion Bonding in Bimetal Ti/Al. *Phys. Met. Metallogr.* **2019**, *120*, 260–268. [CrossRef]
65. Metallurgica, C.W. The Evaluation of Data Obtained with Diffusion Couples of Binary Single-Phase and Multiphase Systems. *Acta Metall.* **1969**, *17*, 99–107. [CrossRef]
66. O, M.; Kajihara, M. Kinetics of Solid-State Reactive Diffusion between Au and Al. *Mater. Trans.* **2011**, *52*, 677–684. [CrossRef]
67. Furuto, A.; Transactions, M.K. Numerical Analysis for Kinetics of Reactive Diffusion Controlled by Boundary and Volume Diffusion in a Hypothetical Binary System. *Mater. Trans.* **2008**, *49*, 294–303. [CrossRef]
68. Mehrer, H. Diffusion in Solids: Fundamentals, Methods, Materials, Diffusion-Controlled Processes. 2007. Available online: https://books.google.com/books?hl=en&lr=&id=IUZVffQLFKQC&oi=fnd&pg=PA27&ots=66n4tPS5ar&sig=lryF-65BupepyceifHOBuR2tNVM (accessed on 8 August 2023).
69. Kundu, J.; Chakraborty, A.; Kundu, J. Bonding Pressure Effects on Characteristics of Microstructure, Mechanical Properties, and Mass Diffusivity of Ti-6Al-4V and TiAlNb Diffusion-Bonded Joints. *Weld. World* **2020**, *64*, 2129–2143. [CrossRef]
70. Kadhim, Z.; Al-Azzawi, A.; And, S.A.-J. Effect of the Diffusion Bonding Conditions on Joints Strength. *J. Eng. Sustain. Dev.* **2009**, *13*, 179–188. Available online: https://www.iasj.net/iasj/download/00f1cf144d5bc71d (accessed on 8 August 2023).
71. Elsa, M.; Khorram, A.; Ojo, O.O.; Paidar, M. Effect of Bonding Pressure on Microstructure and Mechanical Properties of Aluminium/Copper Diffusion-Bonded Joint. *Sadhana-Acad. Proc. Eng. Sci.* **2019**, *44*, 1–9. [CrossRef]
72. Song, T.F.; Jiang, X.S.; Shao, Z.Y.; Fang, Y.J.; Mo, D.F.; Zhu, D.G.; Zhu, M.H. Microstructure and Mechanical Properties of Vacuum Diffusion Bonded Joints between Ti-6Al-4V Titanium Alloy and AISI316L Stainless Steel Using Cu/Nb Multi-Interlayer. *Vacuum* **2017**, *145*, 68–76. [CrossRef]
73. Huang, L.; Sheng, G.; Li, J.; Huang, G.; South, X.Y. Partial Transient-Liquid-Phase Bonding of TiC Cermet to Stainless Steel Using Impulse Pressuring with Ti/Cu/Nb Interlayer. *J. Cent. South Univ.* **2018**, *25*, 1025–1032. [CrossRef]
74. Jia, L.; Engineering, S.G. Diffusion Bonding of TiC Cermet to Stainless Steel Using Impulse Pressuring with Ti-Nb Interlayer. *Rare Met. Mater. Eng.* **2017**, *46*, 882–887. [CrossRef]
75. Wang, F.L.; Sheng, G.M.; Deng, Y.Q. Impulse Pressuring Diffusion Bonding of Titanium to 304 Stainless Steel Using Pure Ni Interlayer. *Rare Met.* **2016**, *35*, 331–336. [CrossRef]
76. Yuan, X.; Tang, K.; Deng, Y.; Luo, J.; Sheng, G. Impulse Pressuring Diffusion Bonding of a Copper Alloy to a Stainless Steel with/without a Pure Nickel Interlayer. *Mater. Des.* **2013**, *52*, 359–366. [CrossRef]
77. Yuan, X.J.; Sheng, G.M.; Luo, J.; Li, J. Microstructural Characteristics of Joint Region during Diffusion-Brazing of Magnesium Alloy and Stainless Steel Using Pure Copper Interlayer. *Trans. Nonferrous Met. Soc. China* **2013**, *23*, 599–604. [CrossRef]
78. Sharma, G.; Dwivedi, D.K. Effect of Pressure Pulsation on Bond Interface Characteristics of 409 Ferritic Stainless Steel Diffusion Bonds. *Vacuum* **2017**, *146*, 152–158. [CrossRef]
79. Cooke, K. Kinetics of Joint Formation During Diffusion Induced Solid State Bonding of Titanium and Magnesium Alloys. In Proceedings of the 18th LACCEI International Multi-Conference for Engineering, Education and Technology, Virtual, 27–31 July 2020.
80. Cooke, K.; Processing, A.A. Current Trends in Dissimilar Diffusion Bonding of Titanium Alloys to Stainless Steels, Aluminium and Magnesium. *J. Manuf. Mater. Process.* **2020**, *4*, 39. [CrossRef]
81. Gao, W.; Xing, S.; Lei, J. Effect of Bonding Temperature and Holding Time on Properties of Hollow Structure Diffusion Bonded Joints of TC4 Alloy. *SN Appl. Sci.* **2020**, *2*. [CrossRef]
82. Chen, B.; Zhu, H.; Zhao, K.; Song, Y.; Liu, D.; Song, X. Effect of Bonding Time on the Microstructure and Mechanical Properties of Graphite/Cu-Bonded Joints. *Rev. Adv. Mater. Sci.* **2021**, *60*, 957–965. [CrossRef]
83. Li, S.X.; Tu, S.T.; Xuan, F.Z. A Probabilistic Model for Prediction of Bonding Time in Diffusion Bonding. *Mater. Sci. Eng. A* **2005**, *407*, 250–255. [CrossRef]
84. Wang, A.; Ohashi, O.; Ueno, K. Effect of Surface Asperity on Diffusion Bonding. *Mater. Trans.* **2006**, *47*, 179–184. [CrossRef]
85. Zhu, L.; Xue, X.; Tang, B.; Kou, H. The Influence of Surface Roughness on Diffusion Bonding of High Nb Containing TiAl Alloy. *Annu. Int. Conf. Adv. Mater. Eng.* 2016, pp. 635–643. Available online: https://www.atlantis-press.com/article/25857962.pdf (accessed on 8 August 2023).
86. Li, B.; Zhang, Z.; Shen, Y.; Hu, W.; Luo, L. Dissimilar Friction Stir Welding of Ti–6Al–4V Alloy and Aluminum Alloy Employing a Modified Butt Joint Configuration: Influences of Process Variables on the Weld Interfaces and Tensile Properties. *Mater. Des.* **2014**, *53*, 838–848. [CrossRef]
87. Scott, M.; Knowlson, P. The Welding and Brazing of the Refractory Metals Niobium, Tantalum, Molybdenum and Tungsten—a Review. *J. Less Common Met.* **1963**, *5*, 205–244. [CrossRef]
88. Moss, T.A.; Davies, R.L.; Barna, G.J. Recent Advances in Refractory Alloys for Space Power System. *NASA Spec* **1969**, *245*, 1. Available online: https://digital.library.unt.edu/ark:/67531/metadc1028911/m2/1/high_res_d/4731743.pdf (accessed on 8 August 2023).
89. Olson, D.L.; Mishra, B.; Wenman, D.W. Welding, Brazing and Joining of Refractory Metals and Alloys. *Miner. Process. Extr. Metall. Rev.* **2008**, *22*, 1–23. [CrossRef]
90. Cadden, C.H.; Odegard, B.C. Refractory Metal Joining for First Wall Applications. *J. Nucl. Mater.* **2000**, *283–287*, 1253–1257. [CrossRef]
91. Qu, D.; Zhou, Z.; Tan, J.; Aktaa, J. Characterization of W/Fe Functionally Graded Materials Manufactured by Resistance Sintering under Ultra-High Pressure. *Fusion Eng. Des.* **2015**, *91*, 21–24. [CrossRef]

92. Basuki, W.W.; Aktaa, J. Investigation on the Diffusion Bonding of Tungsten and EUROFER97. *J. Nucl. Mater.* **2011**, *417*, 524–527. [CrossRef]
93. Oono, N.; Noh, S.; Iwata, N.; Nagasaka, T.; Kasada, R.; Kimura, A. Microstructures of Brazed and Solid-State Diffusion Bonded Joints of Tungsten with Oxide Dispersion Strengthened Steel. *J. Nucl. Mater.* **2011**, *417*, 253–256. [CrossRef]
94. Wang, S.; Ling, Y.; Wang, J.; Xu, G. Microstructure and Mechanical Properties of W/Cu Vacuum Diffusion Bonding Joints Using Amorphous Fe–W Alloy as Interlayer. *Vacuum* **2015**, *114*, 58–65. [CrossRef]
95. Kawakami, Y.; Tamai, F.; Enjoji, T.; Takashima, K. Preparation of Tungsten Carbide/Stainless Steel Functionally Graded Materials by Pulsed Current Sintering. *Solid State Phenom.* **2007**, *127*, 179–184. [CrossRef]
96. Thoma, D.J. Intermetallics: Laves Phases. *Encycl. Mater. Sci. Technol.* **2001**, 4205–4213. [CrossRef]
97. Kong, Y.; Shen, L.; Shen, Y.; Chen, Z. Interfacial Effect on Strengthening Nanoscale Metallic Multilayers—A Combined Hall-Petch Relation and Atomistic Simulation Study. *Mater. Sci. Eng. A* **2016**, *663*, 29–37. [CrossRef]
98. Ebhota, W.S.; Jen, T.-C. Intermetallics Formation and Their Effect on Mechanical Properties of Al-Si-X Alloys. *Intermet. Compd.-Form. Appl.* **2018**. [CrossRef]
99. Kundu, S.; Sam, S.; Chatterjee, S. Evaluation of Interface Microstructure and Mechanical Properties of the Diffusion Bonded Joints of Ti–6Al–4V Alloy to Micro-Duplex Stainless Steel. *Mater. Sci. Eng. A* **2011**, *528*, 4910–4916. [CrossRef]
100. Klueh, R.L.; Cheng, E.T.; Grossbeck, M.L.; Bloom, E.E. Impurity Effects on Reduced-Activation Ferritic Steels Developed for Fusion Applications. *J. Nucl. Mater.* **2000**, *280*, 353–359. [CrossRef]
101. Huang, Q.; Li, J.; Chen, Y. Study of Irradiation Effects in China Low Activation Martensitic Steel CLAM. *J. Nucl. Mater.* **2004**, *329–333*, 268–272. [CrossRef]
102. Tanigawa, H.; Someya, Y.; Sakasegawa, H.; Hirose, T.; Ochiai, K. Radiological Assessment of the Limits and Potential of Reduced Activation Ferritic/Martensitic Steels. *Fusion Eng. Des.* **2014**, *89*, 1573–1578. [CrossRef]
103. Elrefaey, A.; Tillmann, W. Solid State Diffusion Bonding of Titanium to Steel Using a Copper Base Alloy as Interlayer. *J. Mater. Process. Technol.* **2009**, *209*, 2746–2752. [CrossRef]
104. Yu, X.F.; Zheng, D.Y.; Yang, X.F.; Wang, S.Y.; An, M.; Yan, G.B.; Xia, Y.Z.; Xing, F. Effect of Carbide Precipitation Behavior at High Temperatures on Microstructure and Mechanical Properties of M50 Steel. *J. Mater. Res. Technol.* **2022**, *18*, 1155–1165. [CrossRef]
105. Sun, R.; ZHANG, J.; HUANG, X. Influence of Transition Metal V+Cu on Properties of Diffusion Bonding of Ti and Stainless Steel. *Weld. Join.* **1997**, *2*, 22–26.
106. Onozuka, M.; Hirai, S.; Kikuchi, K.; Oda, Y.; Shimizu, K. Manufacturing Study of Be, W and CFC Bonded Structures for Plasma-Facing Components. *J. Nucl. Mater.* **2004**, *329–333*, 1553–1557. [CrossRef]
107. Yang, Z.; Shen, Y.; Wang, Z.; China, J.C. Tungsten/Steel Diffusion Bonding Using Cu/W–Ni/Ni Multi-Interlayer. *Trans. Nonferrous Met. Soc. China* **2014**, *24*, 2554–2558. [CrossRef]
108. Cai, Q.; Liu, W.; Ma, Y.; Liu, H. Microstructure, Residual Stresses and Mechanical Properties of Diffusion Bonded Tungsten–Steel Joint Using a V/Cu Composite Barrier Interlayer. *Int. J. Refract. Met. Hard Mater.* **2015**, *48*, 312–317. [CrossRef]
109. Huang, Y.; Zha, Y.; Zhou, X.; Li, X.; Li, W.; Guo, Q.; Chen, W.; Peng, D. Evolution of Interfacial Structure of the Joints between a Tungsten-Copper Composite and Austenitic Stainless Steel. *Mater. Res. Express* **2021**, *8*, 16514. [CrossRef]
110. Zhang, J.; Xie, D.; Li, Q.; Jiang, C.; Li, Q. Effect of Holding Time on the Microstructure and Strength of Tungsten/Steel Joints by HIP Diffusion Bonded Using a Cu Interlayer. *Mater. Lett.* **2020**, *261*, 126875. [CrossRef]
111. Sun, H.; Han, Y.; Li, Y. Microstructure and Strength of Diffusion Bonding W Alloy/304 Stainless Steel Joint Using a Cu Interlayer. *Int. J. Refract. Met. Hard Mater.* **2023**, *113*, 106188. [CrossRef]
112. Jacobson, D.M.; Humpston, G. *Principles of Brazing*; ASM International: Materials Park, OH, USA, 2005; ISBN 0871708124.
113. Liu, W.; Wang, Z.; Ma, Y.; Cai, Q. Investigation of Tungsten/Steel Brazing Using Ta and Cu Interlayer. *Fusion Eng. Des.* **2016**, *113*, 102–108. [CrossRef]
114. Nath, P.; Chopra, K.L. Thermal Conductivity of Copper Films. *Thin Solid Films* **1974**, *20*, 53–62. [CrossRef]
115. Liu, A.; Wang, L.; Pan, L.; Cheng, X. Microstructure and Mechanical Properties of a Novel High-Density Steel Having High Tungsten Content. *Mater. Sci. Eng. A* **2021**, *824*, 141797. [CrossRef]
116. Stein, F.; Leineweber, A. Laves Phases: A Review of Their Functional and Structural Applications and an Improved Fundamental Understanding of Stability and Properties. *J. Mater. Sci.* **2020**, *56*, 5321–5427. [CrossRef]
117. Zhong, Z.; Hinoki, T.; Kohyama, A. Effect of Holding Time on the Microstructure and Strength of Tungsten/Ferritic Steel Joints Diffusion Bonded with a Nickel Interlayer. *Mater. Sci. Eng. A* **2009**, *518*, 167–173. [CrossRef]
118. Feng, K.; Chen, H.; Xiong, J.; Guo, Z. Investigation on Diffusion Bonding of Functionally Graded WC–Co/Ni Composite and Stainless Steel. *Mater. Des.* **2013**, *46*, 622–626. [CrossRef]
119. Liu, W.S.; Cai, Q.S.; Ma, Y.Z.; Wang, Y.Y.; Liu, H.Y.; Li, D.X. Microstructure and Mechanical Properties of Diffusion Bonded W/Steel Joint Using V/Ni Composite Interlayer. *Mater. Charact.* **2013**, *86*, 212–220. [CrossRef]
120. Cai, Q.; Liu, W.; Ma, Y.; Zhu, W.; Pang, X. Influence of Intermetallic Compounds on the Microstructure and Strength Properties of Diffusion Bonded W–Steel Joints Using Ti/Ni Composite Interlayer. *Fusion Eng. Des.* **2018**, *132*, 110–118. [CrossRef]
121. Villars, P.; Calvert, L.D. *Pearson's Handbook of Crystallographic Data for Intermetallic Phases*; American Society for Metals: Metals Park, OH, USA, 1985. [CrossRef]
122. Cury, R.; Joubert, J.M.; Tusseau-Nenez, S.; Leroy, E.; Allavena-Valette, A. On the Existence and the Crystal Structure of Ni4W, NiW and NiW2 Compounds. *Intermetallics* **2009**, *17*, 174–178. [CrossRef]

123. Gao, Y.; Wang, Z.; Liu, Y.; Li, W.; Liu, C.; Li, H. Diffusion Bonding of 9Cr Martensitic/Ferritic Heat-Resistant Steels with an Electrodeposited Ni Interlayer. *Metals* **2018**, *8*, 1012. [CrossRef]
124. Chen, B.; Li, X.; Cui, H.; Hua, P.; Chen, Y.; Wang, C.; Wu, Y.; Zhou, W. Investigation of Tungsten/MA956 Steel Diffusion Bonding with an Nb/Ni Composite Interlayer. *Int. J. Mod. Phys. B* **2020**, *34*. [CrossRef]
125. Wang, Y.; Chen, S.; Yang, J.; Huang, J.; Chen, S.; Ye, Z. Microstructure, Properties, and Formation Mechanisms of Tungsten/Steel Hot Isostatic Pressing Diffusion Bonding Joint Utilizing a Ni-Si-B Interlayer. *J. Mater. Process. Technol.* **2022**, *299*, 117303. [CrossRef]
126. Yang, Z.; Zhang, X.; Cheng, J.; Li, X.; Shen, Y. Effect of Bonding Process on the Microstructures and Strength of W/Steel Joints with a W-Cu-Ni Interlayer. *Int. J. Refract. Met. Hard Mater.* **2022**, *106*, 105846. [CrossRef]
127. Li, H.; Zhang, H.; Li, G.; Zhao, D.; Jiang, Z. Effects of Holding Time on Interface Microstructure and Element Diffusion of WC-Co-Ni/Stainless Steel Composites. *Int. J. Refract. Met. Hard Mater.* **2022**, *108*, 105951. [CrossRef]
128. Chen, W.Y.; Li, M. Helium Bubble Formation in Nickel under In-Situ Krypton and Helium Ions Dual-Beam Irradiation. *J. Nucl. Mater.* **2022**, *558*, 153342. [CrossRef]
129. Zhu, Z.; Huang, H.; Liu, J.; Zhu, Z. Helium-Induced Damage Behavior in High Temperature Nickel-Based Alloys with Different Chemical Composition. *J. Nucl. Mater.* **2020**, *541*, 152419. [CrossRef]
130. Agarwal, D.C.; Brill, U. High-Temperature-Strength Nickel Alloy. *Adv. Mater. Process.* **2000**, *158*, 31.
131. Dak, G.; Pandey, C. A Critical Review on Dissimilar Welds Joint between Martensitic and Austenitic Steel for Power Plant Application. *J. Manuf. Process.* **2020**, *58*, 377–406. [CrossRef]
132. Zhong, Z.; Hinoki, T.; Nozawa, T.; Park, Y.H.; Kohyama, A. Microstructure and Mechanical Properties of Diffusion Bonded Joints between Tungsten and F82H Steel Using a Titanium Interlayer. *J. Alloys Compd.* **2010**, *489*, 545–551. [CrossRef]
133. Kazakov, N. *Diffusion Bonding of Materials*; Elsevier: Amsterdam, The Netherlands, 1985.
134. Rosiński, M.; Kruszewski, M.J.; Michalski, A.; Fortuna-Zaleśna, E.; Ciupiński, Ł.; Kurzydłowski, K.J. W/Steel Joint Fabrication Using the Pulse Plasma Sintering (PPS) Method. *Fusion Eng. Des.* **2011**, *86*, 2573–2576. [CrossRef]
135. Chen, H.Y.; Luo, L.M.; Zhang, J.; Zan, X.; Zhu, X.Y.; Luo, G.N.; Wu, Y.C. Investigation on W/Fe Diffusion Bonding Using Ti Foil and Ti Powder Interlayer by SPS. *J. Nucl. Mater.* **2015**, *467*, 566–571. [CrossRef]
136. Mizutani, U. *The Hume-Rothery Rules for Structurally Complex Alloy Phases*; CRC Press: Boca Raton, FL, USA, 2010; pp. 323–399. [CrossRef]
137. Noto, H.; Kimura, A.; Kurishita, H.; Matsuo, S.; Nogami, S. Evaluation of Feasibility of Tungsten/Oxide Dispersion Strengthened Steel Bonding with Vanadium Insert. *Mater. Trans.* **2013**, *54*, 451–455. [CrossRef]
138. Zhang, Y.; Sun, D.Q.; Gu, X.Y.; Li, H.M. A Hybrid Joint Based on Two Kinds of Bonding Mechanisms for Titanium Alloy and Stainless Steel by Pulsed Laser Welding. *Mater. Lett.* **2016**, *185*, 152–155. [CrossRef]
139. Song, T.F.; Jiang, X.S.; Shao, Z.Y.; Mo, D.F.; Zhu, D.G.; Zhu, M.H.; Young, C.H.; Luo, Z.P. Interfacial Microstructure and Mechanical Properties of Diffusion-Bonded Joints of Titanium TC4 (Ti-6Al-4V) and Kovar (Fe-29Ni-17Co) Alloys. *J. Iron Steel Res. Int.* **2017**, *24*, 1023–1031. [CrossRef]
140. Liu, W.; Pang, X.; Cai, Q.; Ma, Y.; Zhu, W. Fabrication of W/Steel Joint Using Hot Isostatic Pressing with Ti/Cu/Ti Liquid Forming Interlayer. *Fusion Eng. Des.* **2018**, *135*, 59–64. [CrossRef]
141. Shanmugarajan, B.; Padmanabham, G. Fusion Welding Studies Using Laser on Ti–SS Dissimilar Combination. *Opt. Lasers Eng.* **2012**, *50*, 1621–1627. [CrossRef]
142. Dey, H.C.; Ashfaq, M.; Bhaduri, A.K.; Rao, K.P. Joining of Titanium to 304L Stainless Steel by Friction Welding. *J. Mater. Process. Technol.* **2009**, *209*, 5862–5870. [CrossRef]
143. Miriyev, A.; Stern, A.; Tuval, E.; Kalabukhov, S.; Hooper, Z.; Frage, N. Titanium to Steel Joining by Spark Plasma Sintering (SPS) Technology. *J. Mater. Process. Technol.* **2013**, *213*, 161–166. [CrossRef]
144. Ting, W.; Zhang, B.; Chen, G.; Feng, J.; Qi, T. Electron Beam Welding of Ti-15-3 Titanium Alloy to 304 Stainless Steel with Copper Interlayer Sheet. *Trans. Nonferrous Met. Soc. China* **2010**, *20*, 1829–1834.
145. Chen, S.; Zhang, M.; Huang, J.; Cui, C.; Zhang, H.; Zhao, X. Microstructures and Mechanical Property of Laser Butt Welding of Titanium Alloy to Stainless Steel. *Mater. Des.* **2014**, *53*, 504–511. [CrossRef]
146. Ghosh, M.; Chatterjee, S. Characterization of Transition Joints of Commercially Pure Titanium to 304 Stainless Steel. *Mater. Charact.* **2002**, *48*, 393–399. [CrossRef]
147. Chan, K.; Tjong, S. Effect of Secondary Phase Precipitation on the Corrosion Behavior of Duplex Stainless Steels. *Corros. Mater.* **2014**, *7*, 5268–5304. [CrossRef] [PubMed]
148. Sieurin, H.; Sandström, R. Sigma Phase Precipitation in Duplex Stainless Steel 2205. *Mater. Sci. Eng. A* **2007**, *444*, 271–276. [CrossRef]
149. Murray, J.L. Phase Diagram of Titanium Alloys. *ASM Int.* **1987**, *182*, 340–345.
150. Gräning, T.; Tan, L.; Robin, I.; Katoh, Y.; Yang, Y. A Novel Design of Transitional Layer Structure Between Reduced Activation Ferritic Martensitic Steels and Tungsten for Plasma Facing Materials. *J. Mater. Res. Technol.* **2023**, *24*, 4285–4299. [CrossRef]
151. Jones, R.H.; Leonard, B.R., Jr.; Johnson, A.B., Jr. Assessment of Titanium Alloys for Fusion Reactor First-Wall and Blanket Applications. Final Report; 1980. Available online: https://www.osti.gov/biblio/5171710 (accessed on 8 August 2023).
152. Chakin, V.; Rolli, R.; Gaisin, R.; Hoeppener-Kramar, U.; Nakamichi, M.; Zmitko, M. Tritium Release and Retention in Beryllium and Titanium Beryllide after Neutron Irradiation up to Damage Doses of 23-38 Dpa. *Fusion Eng. Des.* **2020**, *161*, 111938. [CrossRef]

153. Basuki, W.W.; Aktaa, J. Diffusion Bonding between W and EUROFER97 Using V Interlayer. *J. Nucl. Mater.* **2012**, *429*, 335–340. [CrossRef]
154. Kwok, T.; Worsnop, F.; Douglas, J.; Dye, D. Carbon in Solution and the Charpy Impact Performance of Medium Mn Steels. *arXiv* **2023**, arXiv:2301.01190.
155. Basuki, W.W.; Dahm, R.; Aktaa, J. Thermomechanical Analysis of Diffusion-Bonded Tungsten/EUROFER97 with a Vanadium Interlayer. *J. Nucl. Mater.* **2014**, *455*, 635–639. [CrossRef]
156. Basuki, W.W.; Aktaa, J. Process Optimization for Diffusion Bonding of Tungsten with EUROFER97 Using a Vanadium Interlayer. *J. Nucl. Mater.* **2015**, *459*, 217–224. [CrossRef]
157. Habainy, J.; Dai, Y.; Lee, Y.; Iyengar, S. Thermal Diffusivity of Tungsten Irradiated with Protons up to 5.8 Dpa. *J. Nucl. Mater.* **2018**, *509*, 152–157. [CrossRef]
158. Pelleg, J. Diffusion in the Vanadium System. *Philos. Mag. J. Theor. Exp. Appl. Phys.* **2006**, *36*, 725–732. [CrossRef]
159. Wang, P.; Li, Z.; Lin, G.; Zhou, S.; Yang, C.; Yong, Q. Influence of Vanadium on the Microstructure and Mechanical Properties of Medium-Carbon Steels for Wheels. *Metals* **2018**, *8*, 978. [CrossRef]
160. Chung, H.; Loomis, B.; Smith, D. Properties of V-4Cr-4Ti for Application as Fusion Reactor Structural Components. *Fusion Eng. Des.* **1995**, 455–464. [CrossRef]
161. Basuki, W.W.; Aktaa, J. Investigation of Tungsten/EUROFER97 Diffusion Bonding Using Nb Interlayer. *Fusion Eng. Des.* **2011**, *86*, 2585–2588. [CrossRef]
162. Yang, G.; Ma, D.; Liu, L.; Rong, J.; Yu, X. Thermal Diffusion Bonding of Pure Titanium to 304 Stainless Steel Using Aluminum Interlayer. *Chem. Eng. Trans.* **2017**, *59*, 1045–1050. [CrossRef]
163. Wang, Q.; Chen, G.; Wang, K.; Fu, X.; Zhou, W. Enhanced TiAl/Ti3SiC2 Diffusion Bonding by Introducing Amorphous Intergranular Films in Ti3SiC2 through Al Doping. *Scr. Mater.* **2020**, *178*, 493–497. [CrossRef]
164. Zhu, W.; Liu, W.; Ma, Y.; Cai, Q.; Wang, J.; Duan, Y. Microstructural Characteristics, Mechanical Properties and Interfacial Formation Mechanism of Tungsten Alloy/Steel Composite Structure Fabricated by HIP Co-Sintering. *Mater. Des.* **2021**, *211*, 110127. [CrossRef]
165. Liu, W.; Sheng, Q.; Ma, Y.; Cai, Q.; Wang, J.; Liu, Y. Interfacial Microstructures, Residual Stress and Mechanical Analysis of Hot Isostatic Pressing Diffusion Bonded Joint of 93W–4.9Ni–2.1Fe Alloy and 30CrMnSiNi2A Steel. *Fusion Eng. Des.* **2020**, *156*, 111602. [CrossRef]
166. Heuer, S.; Li, B.S.; Armstrong, D.E.J.; Zayachuk, Y.; Linsmeier, C. Microstructural and Micromechanical Assessment of Aged Ultra-Fast Sintered Functionally Graded Iron/Tungsten Composites. *Mater. Des.* **2020**, *191*, 108652. [CrossRef]
167. Yang, Z.; Zhang, X.; Cheng, J.; Li, X.; Shen, Y. Investigation on Hybrid Bonding of Tungsten/Steel with in-Situ Formed Composites Interlayer. *Mater. Today Commun.* **2023**, *35*, 105642. [CrossRef]
168. Zhang, M.; Zhu, W.; Meng, S.; Liu, W.; Ma, Y.; Wang, J.; Sun, H.; Cai, Q. Interfacial Microstructure and Mechanical Properties of Tungsten Alloy/Steel Diffusion Bonding Joint Using CrFeCoNiCu High Entropy Alloy Interlayer. *Mater. Charact.* **2023**, *199*, 112837. [CrossRef]
169. Qi, Q.; Ren, J.Y.; Yue, Y.L.; Gu, Z.E.; Zhu, Y.X.; Wang, C.F. Benefits of High Entropy Alloy Interlayer in the Vacuum Diffusion Bonding of W-CLAM Steel. *Vacuum* **2023**, *214*, 112213. [CrossRef]
170. Lu, C.; Wang, Y.; Yang, M.; Han, Y.; Yang, J.; Huang, J.; Chen, S.; Ye, Z.; Zhao, Y. Interfacial Microstructure and Strengthening Mechanism of W/Steel Diffusion Bonding Joint Using a Porous NiFeWss Interlayer Prepared by in-Situ Reduction. *Mater. Lett.* **2022**, *310*, 131501. [CrossRef]
171. Ganesh, V.; Dorow-Gerspach, D.; Bram, M.; Linsmeier, C.; Matejicek, J.; Vilemova, M. High Heat Flux Testing of Graded W-Steel Joining Concepts for the First Wall. *Energies* **2023**, *16*, 3664. [CrossRef]
172. Lu, C.; Wang, Y.; Lei, X.; Yang, J.; Huang, J.; Chen, S.; Zhao, Y. Influence of Fe-W Intermetallic Compound on Fracture Behavior of Steel/Tungsten HIP Diffusion Bonding Joint: Experimental Investigation and First-Principles Calculation. *J. Manuf. Process.* **2020**, *55*, 131–142. [CrossRef]
173. Chen, L.; Zhang, C.; Guo, Z.; Liu, G. Monitoring the Evolution of Resistance-Welded WC-10Co/B318 Steel Joint Based on Welding Time. *Int. J. Refract. Met. Hard Mater.* **2023**, *113*, 106221. [CrossRef]
174. Grammes, T.; Emmerich, T.; Qu, D.; Heinze, O.; Vaßen, R.; Aktaa, J. Functionally Graded Tungsten/EUROFER Coating for DEMO First Wall: From Laboratory to Industrial Production. *Fusion Eng. Des.* **2023**, *188*, 113430. [CrossRef]
175. Wei, C.; Liu, L.; Gu, Y.; Huang, Y.; Chen, Q.; Li, Z.; Li, L. Multi-Material Additive-Manufacturing of Tungsten - Copper Alloy Bimetallic Structure with a Stainless-Steel Interlayer and Associated Bonding Mechanisms. *Addit. Manuf.* **2022**, *50*, 102574. [CrossRef]
176. Khedr, M.; Hamada, A.; Järvenpää, A.; Elkatatny, S.; Abd-Elaziem, W. Review on the Solid-State Welding of Steels: Diffusion Bonding and Friction Stir Welding Processes. *Metals* **2022**, *13*, 54. [CrossRef]
177. Chu, Q.; Li, Y.; Cao, Q.; Zhang, M.; Zhao, P.; Yan, F.; Luo, H.; Wang, X.; Yan, C. Microstructure and Mechanical Properties of Cu/Steel Dissimilar Joints. *Int. J. Press. Vessel. Pip.* **2022**, *200*, 104828. [CrossRef]
178. Joshani, E.; Beidokhti, B.; Davodi, A.; Amelzadeh, M. Evaluation of Dissimilar 7075 Aluminum/AISI 304 Stainless Steel Joints Using Friction Stir Welding. *J. Alloys Metall. Syst.* **2023**, *3*, 100017. [CrossRef]
179. Wei, C.; Zhang, H.; Wang, Z.; Wei, Y.; Chen, J. Adverse Effects of Continuous Oxides at the Diffusion Bonding Interface of RAFM Steels and the Improvement of Joint Strength by Bonding Pressure. *Mater. Today Commun.* **2022**, *31*, 103840. [CrossRef]

180. Habibi, F.; Samadi, A.; Nouri, M. Microstructural Evolution during Low-Temperature Brazing of WC-Co Cemented Carbide to AISI 4140 Steel Using a Silver-Based Filler Alloy. *Int. J. Refract. Met. Hard Mater.* **2023**, 106354. [CrossRef]
181. Izaguirre, I.; Roldán, M.; de Prado, J.; Bonache, V.; Sánchez, M.; Ureña, A. S/TEM Examination and Nanomechanical Response of W-Eurofer Joints Brazed with Cu Interlayers. *Nucl. Mater. Energy* **2022**, *31*, 101155. [CrossRef]
182. Tejado, E.; de Prado, J.; Tarancón, S.; Sánchez, M.; Martín, A.; Pastor, J.Y.; Ureña, A. Thermomechanical Characterisation of W-Eurofer 97 Brazed Joints. *J. Nucl. Mater.* **2020**, *542*, 152504. [CrossRef]
183. de Prado, J.; Sal, E.; Sánchez, M.; García-Rosales, C.; Ureña, A. Microstructural and Mechanical Characterization of Self-Passivating W-Eurofer Joints Processed by Brazing Technique. *Fusion Eng. Des.* **2021**, *169*, 112496. [CrossRef]
184. Yamashita, T.; Tokitani, M.; Hamaji, Y.; Shen, J.; Noto, H.; Masuzaki, S.; Muroga, T. Evaluation of Heat Removal Property in W/Cu/RAFM Steel Joint by Using Electron Beam Facility. *Nucl. Mater. Energy* **2022**, *33*, 101236. [CrossRef]
185. Izaguirre, I.; Loewenhoff, T.; de Prado, J.; Sánchez, M.; Wirtz, M.; Díaz-Mena, V.; Ureña, A. Thermal Fatigue Response of W-EUROFER Brazed Joints by the Application of High Heat Flux Loads. *J. Mater. Process. Technol.* **2023**, *319*, 118056. [CrossRef]
186. Liu, K.; Chen, P.; Zhou, Q.; Xiao, C.; Feng, J.; Li, Y.; Qiao, J.; Zhou, Q.; Zhu, L.; Gao, X. Interfacial Evolution Mechanism of W/Cu Explosive Welding Interface Affected by Preheating. *Int. J. Refract. Met. Hard Mater.* **2023**, 106351. [CrossRef]
187. Garcia, J.M.; Monteiro, A.C.A.; Casanova, A.d.M.B.; Checca Huaman, N.R.; Monteiro, S.N.; Brandao, L.P. Microstructural Analysis of Phase Precipitation during High Temperature Creep in AISI 310 Stainless Steel. *J. Mater. Res. Technol.* **2023**, *23*, 5953–5966. [CrossRef]
188. Bahl, S.; Singh, T.; Kumar, V.; Sehgal, S.; Bagha, A.K.; Bahl, S.; Singh, T.; Kumar, V.; Sehgal, S.; Bagha, A.K. A Systematic Review on Recent Progress in Advanced Joining Techniques of the Lightweight Materials. *AIMS Mater. Sci.* **2021**, *8*, 62–81. [CrossRef]
189. Lambiase, F.; Scipioni, S.; Lee, C.; Ko, D.; Materials, F.L. A State-of-the-Art Review on Advanced Joining Processes for Metal-Composite and Metal-Polymer Hybrid Structures. *Materials* **2021**, *14*, 1890. [CrossRef] [PubMed]
190. Ahn, B. Recent Advances in Brazing Fillers for Joining of Dissimilar Materials. *Metals* **2021**, *11*, 1037. [CrossRef]
191. Cai, W.; Daehn, G.; Vivek, A.; Li, J.; Khan, H.; Mishra, R.S.; Komarasamy, M. A State-of-the-Art Review on Solid-State Metal Joining. *J. Manuf. Sci. Eng. Trans. ASME* **2019**, *141*, 031012. [CrossRef]
192. Mishra, R.S.; Ma, Z.Y. Friction Stir Welding and Processing. *Mater. Sci. Eng. R Rep.* **2005**, *50*, 1–78. [CrossRef]
193. Matheny, M.P.; Graff, K.F. Ultrasonic Welding of Metals. *Power Ultrason. Woodhead Publ.* **2015**, 259–293. [CrossRef]
194. Findik, F. Recent Developments in Explosive Welding. *Mater. Des.* **2011**, *32*, 1081–1093. [CrossRef]
195. Cavaliere, P.; Sadeghi, B.; Shabani, A. Spark Plasma Sintering: Process Fundamentals. *Spark Plasma Sinter. Mater.* **2019**, 3–20. [CrossRef]
196. Torralba, J.M. Improvement of Mechanical and Physical Properties in Powder Metallurgy. *Compr. Mater. Process.* **2014**, *3*, 281–294. [CrossRef]
197. Yahiro, Y.; Mitsuhara, M.; Tokunakga, K.; Yoshida, N. Characterization of Thick Plasma Spray Tungsten Coating on Ferritic/Martensitic Steel F82H for High Heat Flux Armor. *J. Nucl. Mater.* **2009**, *386*, 784–788. [CrossRef]
198. Wang, X.G.; Li, X.G.; Wang, C.G. Influence of Diffusion Brazing Parameters on Microstructure and Properties of Cu/Al Joints. *J. Manuf. Process.* **2018**, *35*, 343–350. [CrossRef]
199. Tiwari, G.P.; Mehrotra, R.S.; Iijima, Y. Solid State Diffusion and Bulk Properties. *Diffus. Process. Adv. Technol. Mater.* **2005**, 69–111. [CrossRef]
200. Heuer, S.; Coenen, J.W.; Pintsuk, G.; Matějíč Ek, J.; Vilémová, M.; Linsmeier, C. Overview of Challenges and Developments in Joining Tungsten and Steel for Future Fusion Reactors. *Phys. Scr.* **2020**, *2020*, 014028. [CrossRef]
201. Kaufmann, M.; Neu, R. Tungsten as First Wall Material in Fusion Devices. *Fusion Eng. Des.* **2007**, *82*, 521–527. [CrossRef]
202. Lambiase, F.; Di Ilio, A. Damage Analysis in Mechanical Clinching: Experimental and Numerical Study. *J. Mater. Process. Technol.* **2016**, *230*, 109–120. [CrossRef]
203. Gludovatz, B.; Wurster, S.; Hoffmann, A.; Pippan, R. Fracture Toughness of Polycrystalline Tungsten Alloys. *Int. J. Refract. Met. Hard Mater.* **2010**, *28*, 674–678. [CrossRef]

Disclaimer/Publisher's Note: The statements, opinions and data contained in all publications are solely those of the individual author(s) and contributor(s) and not of MDPI and/or the editor(s). MDPI and/or the editor(s) disclaim responsibility for any injury to people or property resulting from any ideas, methods, instructions or products referred to in the content.